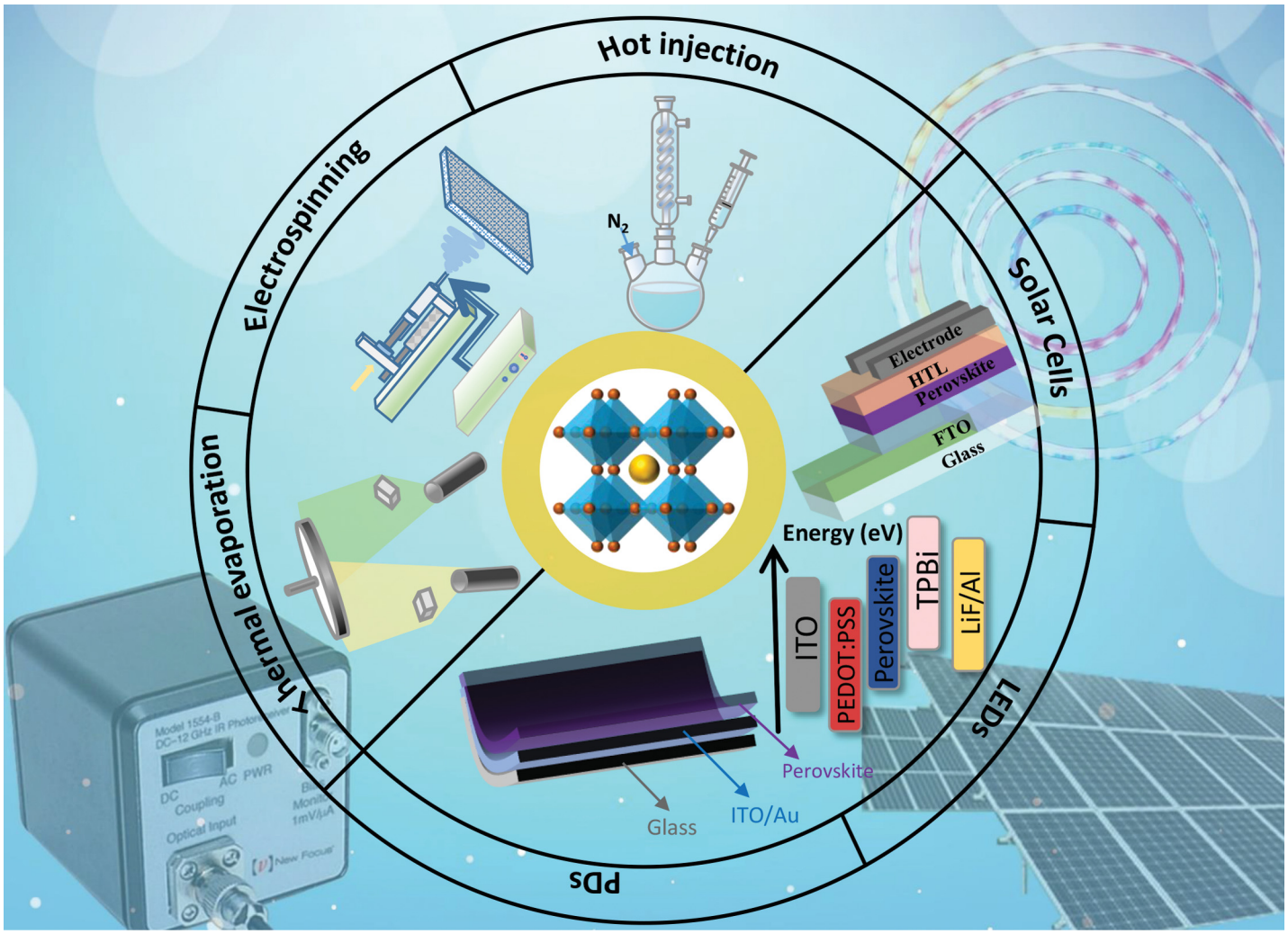

Showcasing research from Professor Yaofang Zhang's laboratory, School of Physical Science and Technology, Tiangong University, Tianjin, China.

Progress in the preparation and application of $CsPbX_3$ perovskites

In recent years, perovskite has become a popular material of increasing interest. All-inorganic perovskites have better stability compared to organic–inorganic metal halide perovskites. Therefore, all-inorganic $CsPbX_3$ (X = Br, I, Cl) perovskites are becoming popular and potential materials suitable for optoelectronic devices. $CsPbX_3$ perovskites exhibited many excellent physical and optical properties, such as high carrier mobility, high fluorescence, *etc.* In this review, the recent progress on the preparation and application of $CsPbX_3$ perovskites is outlined. A brief summary of the full paper is presented and the challenges facing the all-inorganic $CsPbX_3$ perovskites field are discussed.

As featured in:

See Yaofang Zhang *et al.*, *Mater. Adv.*, 2022, **3**, 4053.

ROYAL SOCIETY OF CHEMISTRY

rsc.li/materials-advances

Registered charity number: 207890

Materials Advances

ROYAL SOCIETY OF CHEMISTRY

REVIEW

View Article Online
View Journal | View Issue

Cite this: *Mater. Adv.*, 2022, 3, 4053

Progress in the preparation and application of $CsPbX_3$ perovskites

Yingwen Pan, [ab] Yaofang Zhang,*[ab] Weimin Kang, [ac] Nanping Deng,[ac] Zirui Yan,[ab] Wei Sun,[ab] Xiaoying Kang[ab] and Jian Ni[d]

Received 29th January 2022,
Accepted 7th April 2022

DOI: 10.1039/d2ma00100d

rsc.li/materials-advances

In recent years, organic–inorganic metal halide (OIH) perovskites have become a popular material of increasing interest. Due to the presence of organic cations, OIH perovskites suffer from chemical instability and easy decomposition in harsh environments with high temperature and humidity. All-inorganic perovskites have better stability compared to OIH perovskites. Due to the intensive research and continuous optimization of the preparation process, the power conversion efficiency (PCE) of all-inorganic perovskite solar cells (PSCs) has exceeded 20%. Therefore, all-inorganic $CsPbX_3$ (X = Br, I, Cl) perovskites are becoming popular and are potential materials suitable for optoelectronic devices. $CsPbX_3$ perovskites exhibit many excellent physical and optical properties, such as high carrier mobility and high fluorescence. In this review, recent progress on the preparation and application of $CsPbX_3$ perovskites is outlined. Firstly, the physical structure and excellent optical properties of $CsPbX_3$ perovskites are briefly described. Next, the preparation of different morphologies of $CsPbX_3$ perovskites is described. Furthermore, this paper summarizes the application of $CsPbX_3$ in optoelectronic devices, including PSCs, light-emitting diodes (LEDs), and photodetectors (PDs). The performance parameters of $CsPbX_3$ devices are summarized. Finally, a brief summary of the full paper is presented and the challenges facing the field of all-inorganic $CsPbX_3$ perovskites are discussed.

1. Introduction

OIH perovskites are popular and promising materials that have aroused tremendous public attention due to their excellent photoelectric properties, such as high absorptivity, high carrier mobility, smaller exciton binding energy, and adjustable bandgap.[9–13] Perovskites were originally discovered by a German mineralogist Gustav Rose in 1839; the first discovered perovskite-structure substance was $CaTiO_3$.[14,15] OIH perovskites possess the general molecular formula ABX_3, which is composed of three ions occupying different positions of the crystal lattice. The A site is a monovalent organic cation that has a larger ionic radius, where A = methylammonium ($CH_3NH_3^+$, MA^+) or formamidinium ($CH_3(NH_2)_2^+$, FA^+).[22] The B site is a metal cation whose ionic radius is smaller than that of A, where B = Pb^{2+}, Sn^{2+} or Ge^{2+}.[24] The X site is a halide anion, where X = Cl^-, Br^- or I^-.

Fig. 1a shows the crystal structure of the perovskite $CaTiO_3$ and Fig. 1b shows the crystal structure of OIH perovskites. The A ion occupies the octahedral void and is located in the centre of the cubic cell. The B metal cations are located at the apex of the cubic cell and are surrounded by six halogen anions. Thus, the perovskite has excellent photoelectric properties because of its unique physical structure.

Although OIH perovskites have many outstanding properties, their stability issues greatly limit their application. For instance, they are very sensitive to harsh environments. Due to the

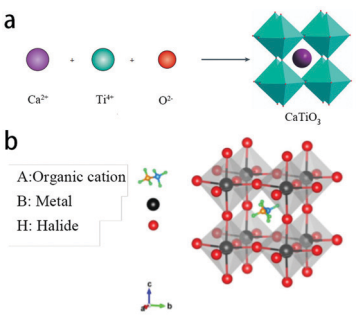

Fig. 1 (a) The crystal structure of the perovskite $CaTiO_3$.[34] Copyright 2017, Springer Nature. (b) The crystal structure of OIH perovskites.[36] Copyright 2020, Walter de Gruyter.

[a] State Key Laboratory of Separation Membranes and Membrane Processes, Tiangong University, Tianjin 300387, P. R. China. E-mail: zhangyaofang@tiangong.edu.cn
[b] School of Physical Science and Technology, Tiangong University, Tianjin 300387, P. R. China
[c] School of Textile Science and Engineering, Tiangong University, Tianjin 300387, P. R. China
[d] Department of Electronic Science and Technology, College of Electronic Information and Optical Engineering, Nankai University, Tianjin, 300350, China

instability of organic cations in OIH perovskites, they decompose easily at high humidity and temperature.[19,24] Xue *et al.* studied the structural properties during the decomposition of $MAPbI_3$ ($MA = CH_3NH_3^+$) by first-principles calculations.[30] The intrinsically poor structural stability of $MAPbI_3$ can cause it to decompose into PbI_2, whether in high humidity or not. In addition, high temperature will cause the perovskite phase transition, which results in instability of the perovskite. For instance, the black perovskite-type (α-phase) of $FAPbI_3$ is stable at high temperatures above 160 °C, but it turns into the yellow δ-phase when exposed to low temperatures and moisture.[40] Moreover, Schwenzer *et al.* investigated the effects of different cation compositions on the thermal stability of perovskite thin films; the surface material composition of $FACsPbI_3$ films was less affected than that of $FAPbI_3$ films after 500 h at 85 °C.[41] The poor thermal and moisture stability of organic–inorganic hybrid perovskite materials is caused by the facile phase transitions and the formation of hydrated phases near room temperature.[43] Kulbak *et al.* explored the thermal stability of $MAPbBr_3$ and $CsPbBr_3$ by thermogravimetric analysis.[44] $MAPbBr_3$ began to decompose at 220 °C, while $CsPbBr_3$ began to decompose at 580 °C; this indicates that all-inorganic perovskites have higher thermal stability than OIH perovskites. Therefore, it is known that all-inorganic perovskites are more stable than OIH perovskites.[45] All-inorganic perovskite nanocrystals (PNCs) have advantages of high photoluminescence quantum yield (PLQY), narrow band emission, and adjustable fluorescence wavelength.[46]

In recent years, increasing numbers of scholars have focused on all-inorganic perovskite materials owing to their unique advantages. The A site in the perovskite general formula can be replaced by an inorganic cation. In a perovskite structure, its structure and stability are determined by the tolerance factor t and octahedral factor μ.[47] In DFT calculations at 0 K, the γ phase is always the most stable, and the most ideal perovskite structure is the α phase, which has a tolerance factor of $t = 1$; however, it is unstable.[48] When $0.81 < t < 1.11$ and $0.44 < \mu < 0.90$, the crystal structure of perovskite is stable.[11] When $t < 0.89$, perovskite is a tetragonal (β-phase) or orthogonal (γ-phase) structure with poor symmetry. The Cs^+ ion can match the requirements of t, and it has replaced organic cations to improve the stability of perovskite in applications.

According to the citation report of American Chemical Society (ACS) Publications, we can conclude that the publications of $CsPbX_3$ have shown an upward trend in the last 10 years. Moreover, the hot injection method was the first to emerge, and in recent years, the new electrospinning method has gradually arisen (Fig. 2). In addition, based on the hot injection method, the PCE of $CsPbX_3$-based PSCs has improved from 5.8% ($CsPbBr_3$) and 2.9% ($CsPbI_3$) to 17.1% ($CsPbI_3$) from the first paper in 2015 to date, and the stability has been continuously improved.[49] Tong *et al.* improved the hot injection method, such as adding zeolite-encapsulated $CsPbX_3$ NCs, doping with Mn^+, and *in situ* growth of $CsPbX_3$ NCs in metal-organic framework crystals, which improved the luminescence efficiency of the materials.[7,17,28,50–57] Zhang *et al.* prepared dense and uniform $CsPbX_3$ thin films by thermal evaporation and applied them in lasers, LEDs, PSCs, and other photoelectric fields.[1,16,35,58–64] In recent years, electrospinning has

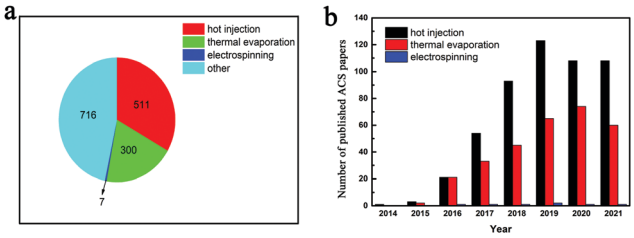

Fig. 2 (a) Number of articles on the three preparation methods of $CsPbX_3$ as percentages of core publications. (b) Statistics of core publications based on $CsPbX_3$ preparation methods.

emerged as a new method to prepare $CsPbX_3$. Huang *et al.* encapsulated $CsPbX_3$ NCs in different polymers and prepared $CsPbX_3$ nanofibers by electrospinning.[5,19,46,65–70]

Here, in this review, we will describe the latest progress of $CsPbX_3$ perovskites and their applications in optoelectronic devices. The synthesis of $CsPbX_3$ perovskites in different morphologies, including single crystals, thin films and nanocrystals, are first described. Then, the optoelectronic applications of $CsPbX_3$ perovskite are reviewed, including PSCs, LEDs, and PDs. Finally, the challenges and prospects of the $CsPbX_3$ perovskites are discussed.

2. Synthesis of $CsPbX_3$ perovskites

To explore the characteristics of $CsPbX_3$ perovskites and the application of different optoelectronic devices, various synthesis strategies of $CsPbX_3$ perovskites in different morphologies were summarized, such as single crystals, thin films and nanocrystals.

2.1 Synthesis of single crystals

Single crystals of all-inorganic perovskites are typically prepared by the Bridgman growth method. Song *et al.* obtained ultralarge 25 cm^3-volume $CsPbBr_3$ SC ingot through an improved Bridgman growth method using a four-zone furnace.[6] The $CsPbBr_3$ SC was prepared by the reaction of equimolar amounts of CsBr (42.6 g) and $PbBr_2$ (73.4 g) in fused silica ampoules. A schematic of the growth is shown in Fig. 3a.

In addition to the traditional Bridgman growth method, the solution growth method has been developed to obtain high-quality perovskite single crystals. Fu *et al.* prepared solution-grown $CsPbBr_3$, $CsPbCl_3$ and their halide alloys of $CsPb(Br,Cl)_3$ with high-quality single crystal nanostructures.[18] Nanoplates and nanocrystals were prepared by reacting PbX_2 and lead acetate films with CsBr (CsCl) solutions with methanol at room temperature. Fig. 3b displays the SEM image of $CsPbBr_3$ NWs grown at room temperature for approximately 15 hours. As shown in Fig. 3c, the photoluminescence (PL) spectrum of $CsPbBr_3$ NW peaked at 530 nm, with a FWHM of 17 nm. Since the direct synthesis of $CsPb(Br,I)_3$ NWs by the solution method is challenging, the low temperature vapor-phase method was developed. As shown in Fig. 3d, $CsPbBr_3$ NWs were successfully converted to $CsPbI_3$ by a low temperature vapor-phase halide exchange process, maintaining the NW morphology and perovskite lattice.

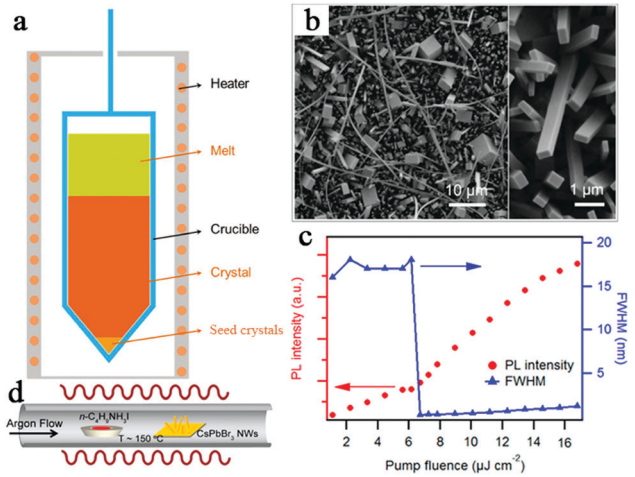

Fig. 3 (a) Schematic diagram of the growth of a crystal by the Bridgeman method.[6] Copyright 2017, John Wiley and Sons Inc. (b) Scanning electron microscope (SEM) image of the $CsPbBr_3$ nanostructure. The inset on the right is a magnified SEM image.[18] (c) Integrated emission intensity and full width at half maximum (FWHM) of the dominant emission peak plotted as a function of P, which shows that the lasing threshold is 6.2 μJ cm^{-2}.[18] (d) Schematic diagram of the vapour conversion of $CsPbBr_3$ nanostructures into $CsPb(Br,I)_3$.[18] Copyright 2016, American Chemical Society.

2.2 Preparation of thin films

Typically, perovskite films can be prepared by the solution method or by thermal evaporation. The thin films prepared by traditional thermal evaporation are compact, uniform and reproducible, and this method can be used to prepare large-area uniform perovskite thin films.[1,60] Thermal evaporation mainly refers to vapor deposition; H. J. Snaith's group at the University of Oxford prepared planar heterojunction perovskite solar cells with 15% PCE using the vapor deposition method for the first time.[1] Fig. 4a illustrates the process of the preparation of $CH_3NH_3PbI_3$-xCl_x thin films by dual-source vapor deposition, in which organic source methylammonium iodide and inorganic source PbI_2 were used for dual-source thermal evaporation.

Liu *et al.* prepared $CsPbBr_3$ perovskite films by dual-source co-evaporation of CsBr and $PbBr_2$ under vacuum conditions.[16] When the substrate temperature was 300 °C and the evaporation rate ratio was 0.7 : 1, the best crystallinity and optimum stoichiometry of the $CsPbBr_3$ films were displayed. In addition, the $CsPbBr_3$ film films annealed at 500 °C had the largest grains, and they were tightly connected, as shown in Fig. 4b and c. This shows that photocarriers can travel to opposite electrodes without crossing through grain boundaries, which yields excellent photovoltaic performance. Fig. 4e and f shows the UV-Vis absorbance spectra of the deposited $CsPbBr_3$ films under different annealing temperatures, and the PL peak of all the films was 520 nm. On this basis, stable planar $CsPbBr_3$ solar cells were prepared with an efficiency of up to 6.95%. This finding suggests that dual-source thermal co-evaporation is an effective method for preparing $CsPbBr_3$ films with excellent properties.

Yang *et al.* prepared $CsPbBr_3$ perovskite films by thermal co-evaporation combined with continuous low-temperature thermal annealing and studied their morphology and crystallization

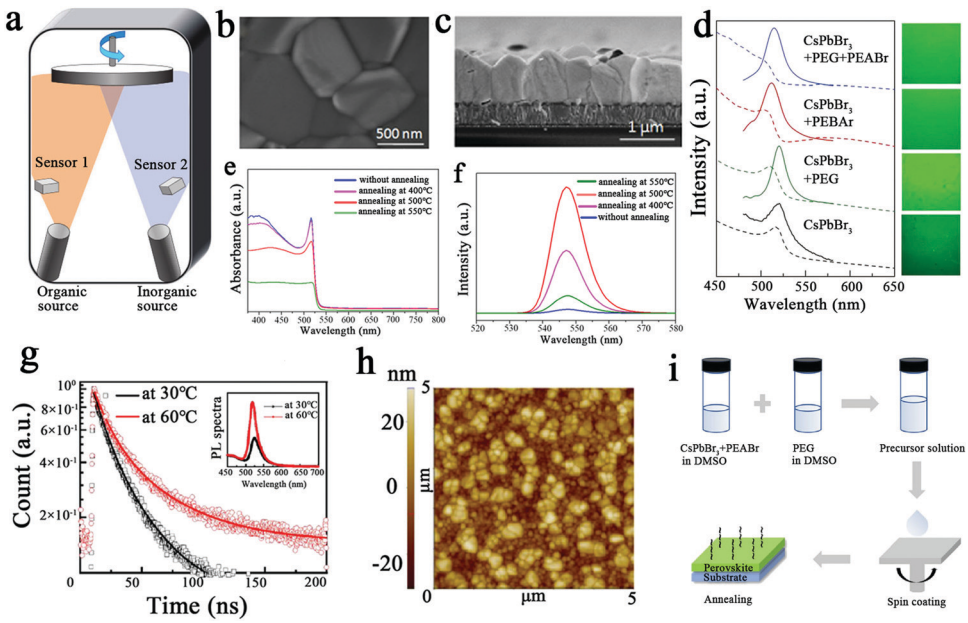

Fig. 4 (a) Schematic diagram of the dual-source thermal evaporation system: the organic source is methylammonium iodide and the inorganic source is PbI_2.[1] Copyright 2013, Springer Nature. (b) Surface SEM images of deposited $CsPbBr_3$ films under annealing at 500 °C.[16] (c) Cross-sectional SEM images of deposited $CsPbBr_3$ films under annealing at 500 °C.[16] (d) Absorption (dashed line) and PL (solid line) spectra of $CsPbBr_3$ films on a quartz substrate.[26] (e) UV-Vis absorption spectra of deposited $CsPbBr_3$ films under different annealing temperatures.[16] (f) PL spectra of deposited $CsPbBr_3$ films under different annealing temperatures.[16] Copyright 2018, Elsevier BV. (g) Time-resolved photoluminescence (TRPL) and steady-state photoluminescence spectroscopy (inset).[35] (h) AFM images of 100 nm thick $CsPbBr_3$ films prepared at 60 °C with deposition rates of 1.0 Å s^{-1}.[35] Copyright 2020, American Chemical Society. (i) Preparation process of $CsPbBr_3$ perovskite thin films.[26] Copyright 2019, John Wiley and Sons Inc.

processes.[35] Dense and uniform $CsPbBr_3$ grains with an average size of 150 ± 74 nm were formed at a standard deposition rate of 1.0 Å s^{-1} at 60 °C. As shown in the inset of Fig. 4g, the steady-state photoluminescence spectra of $CsPbBr_3$ perovskite films prepared at 60 °C is superior to that of films prepared at 30 °C. When the deposition rate is 1.0 Å s^{-1}, a $CsPbBr_3$ film with a smoother surface can be seen under atomic force microscopy (AFM) in Fig. 4h. This article revealed for the first time the regulation of grain size and densification of $CsPbBr_3$ films during thermal co-evaporation fabrication by *in situ* thermal dynamic crystallization.

The general solution method for the preparation of perovskite films is a one-step or two-step spin coating method. Due to the morphological defects and serious non-radiative recombination of all-inorganic perovskite, the efficiency of the device is seriously affected. Tang *et al.* doped two additives, PEABr and polyethylene glycol (PEG), to prepare $CsPbBr_3$ perovskite films using the spin-coating method to passivate defects at the grain boundaries and thus reduce non-radiative recombination.[26] Fig. 4i shows the preparation process of the $CsPbBr_3$ perovskite films with the PEG and PEABr additives. Fig. 4d shows the PL spectra of various $CsPbBr_3$ perovskite films on PEDOT:PSS peaking at 520 nm. This method provides an effective strategy for preparing perovskite thin films with high density and few defects.

2.3 Synthesis of nanocrystals

All-inorganic perovskite nanocrystals can be synthesised by a variety of methods, the most mainstream being hot injection. The hot injection method has been widely used in the synthesis of traditional metal chalcogenide (PbS, CdS, CdSe) nanocrystals, and it is currently widely used for the preparation of quantum dots.[71] Based on the traditional quantum dot synthesis method, efficient luminescent $CsPbX_3$ nanocrystals (NCs) were synthesized by hot injection.[72] In the hot injection method, the precursor solution was injected rapidly into the remaining solution of the synthetic compound under an inert atmosphere and a certain temperature, as can be seen in Fig. 5a.[2,73] For the synthesis of $CsPbX_3$ NCs, the Cs-containing precursor was first injected rapidly into the PbX_2 precursor solution containing the organic ligand at a certain temperature.[74] The precursor solution reacted in a high boiling point solvent with ligand-controlled growth to induce nucleation and obtain uniformly sized $CsPbX_3$ nanocrystals.

In 2015, Kovalenko *et al.* first prepared $CsPbX_3$ (X = Cl, Br, I and halogen mixtures) perovskite nanocrystals using the hot injection method.[17] They prepared $CsPbX_3$ NCs that possess 4–15 nm cubic perovskite crystals. Fig. 5b shows transmission electron microscopy (TEM) images of the $CsPbBr_3$ NCs; the size of the grains is uniformly distributed around 8 nm. As shown in Fig. 5c, the emission spectrum of the $CsPbX_3$ NCs is tunable in the entire visible spectral region of 410–700 nm by varying the ratio of the halides, and the corresponding FWHMs can be measured as 12–42 nm. $CsPbX_3$ NCs have high quantum yields of 50–90% and short radiation lifetimes of 1–29 ns, as can be seen in Fig. 5d. Fig. 5e shows the absorption and emission spectra of $CsPbX_3$.

In recent years, $CsPbX_3$ perovskite quantum dots (PeQDs) have been embedded in intermediate structure metal–organic framework crystals (MOFs) to improve the stability of the PeQDs. In 2018, Wang's group prepared green-emitting $CsPbBr_3$ and red-emitting $CsPbBr_{0.6}I_{2.4}$ PeQDs by hot injection and embedded $CsPbX_3$ PeQDs into intermediate structured zinc-based metal organic-framework (MOF-5) crystals to improve the stability of the PeQDs.[7] The PLQYs of the $CsPbBr_3$/MOF-5 and $CsPbBr_{0.6}I_{2.4}$/MOF-5 composites were 52% and 56%, respectively; these were much higher than the PLQY of pure $CsPbX_3$ powder, indicating that MOF-5 improved the performance of the $CsPbX_3$ PeQDs. The average composite lifetimes of the $CsPbBr_3$/MOF-5 and $CsPbBr_{0.6}I_{2.4}$/MOF-5

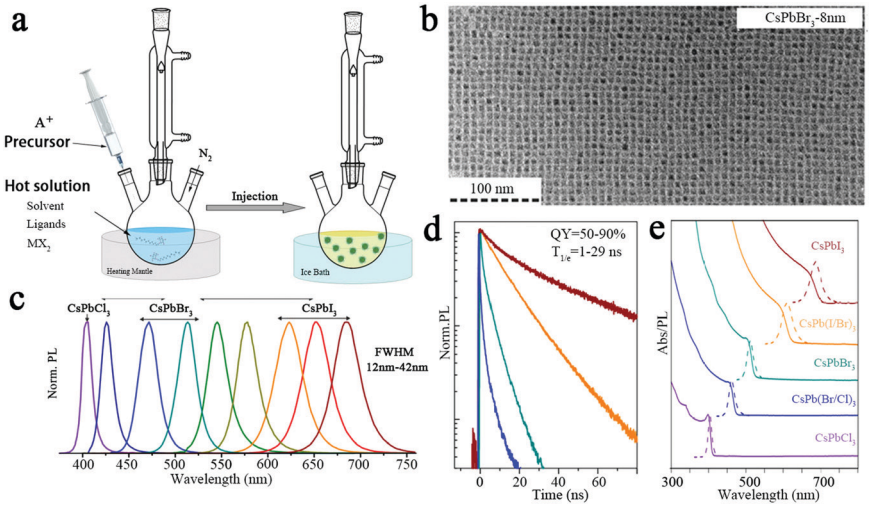

Fig. 5 (a) Schematic diagram of the hot injection method.[2] Copyright 2019, American Chemical Society. (b) TEM images of the $CsPbBr_3$ NCs.[17] (c) PL spectrum of the $CsPbX_3$ NCs.[17] (d) Time-resolved PL decay for all samples shown in (c) except $CsPbCl_3$.[17] (e) Typical optical absorption and PL spectra.[17] Copyright 2015, American Chemical Society.

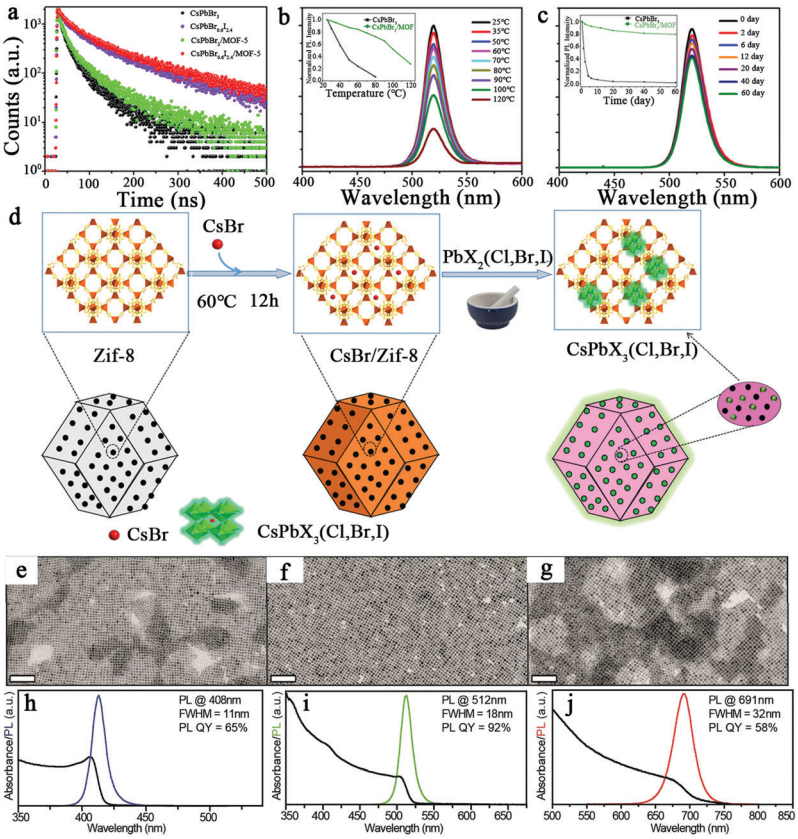

Fig. 6 (a) Time-resolved photoluminescence decay curves of the $CsPbBr_3$ powder, $CsPbBr_{0.6}I_{2.4}$,$CsPbBr_3$/MOF-5 and $CsPbBr_{0.6}I_{2.4}$/MOF-5 composites.[7] (b) Thermal stability test.[7] (c) Long-term storage stability test of $CsPbBr_3$/MOF-5.[7] Copyright 2019, Elsevier. (d) Synthesis of $CsPbX_3$/ZIF-8.[25] Copyright 2021, American Chemical Society. TEM images of (e) $CsPbCl_3$, (f) $CsPbBr_3$, and (g) $CsPbI_3$ NCs. Absorption and PL spectra of (h) $CsPbCl_3$, (i) $CsPbBr_3$, and (j) $CsPbI_3$ NCs dispersed in toluene.[28] Copyright 2018, American Chemical Society.

composites were longer than those of the pure $CsPbX_3$ PeQDs (Fig. 6a). $CsPbBr_3$/MOF-5 maintained 72.8% of its initial PL intensity at 80 °C and could also emit light at 120 °C, which demonstrated the high thermal stability of $CsPbBr_3$/MOF-5 (Fig. 6b). $CsPbBr_3$/MOF-5 maintained 79.2% photoluminescence intensity after 60 days at room temperature, which demonstrated its good long-term storage stability (Fig. 6c). In addition, Zhao *et al.* grew $CsPbX_3$ (X = Cl, Br, and I) QDs *in situ* in zeolitic imidazolate framework-8 (ZIF-8), which improved the stability of the $CsPbX_3$ QDs.[25] The synthesis process of $CsPbX_3$/ZIF-8 is shown in Fig. 6d. Furthermore, ZIF-8 can control the size of $CsPbX_3$ quantum dots. Among them, the PLQY of $CsPbBr_3$/ZIF-8 is up to 72%.

Imran *et al.* replaced the halide precursor PbX_2 (X = Cl, Br or I) salt with benzoyl halide in the hot injection method, which facilitates the injection of the metal cation and the desired ligands into the solution.[28] This method also allows strict control of the size distribution, regulation of the $CsPbX_3$ NC components and high phase purity. Fig. 6e–g shows TEM images of $CsPbX_3$. Fig. 6h–j shows the emission peaks of the PL spectra of $CsPbX_3$ NCs and the narrow FWHMs of the $CsPbX_3$ NCs, from 11 nm (X = Cl) to 18 nm (X = Br) to 32 nm (X = I). In addition, the PLQYs of the $CsPbBr_3$ NCs were up to 92%. The synthesized $CsPbX_3$ NCs showed high phase stability, uniform size distribution, and unprecedented optical properties.

Electrospinning has become a popular method for the preparation of nanofibers in recent years, and it has aroused public attention because of its low cost, easy fabrication process, and fine-tuning of the morphology of fibers, as well as the large specific surface area of the prepared fibers.[5,75] Electrospinning technology is used to prepare nanofibers by overcoming the surface tension of the jet and the internal viscous force by using electrostatic forces as the traction force.[76] A schematic of the electrospinning process is shown in Fig. 7a. The $CsPbBr_3$ NCs were coated with polymer by electrospinning, which improved their water and heat resistance, showing their promising application in optoelectronic devices.

Liao *et al.* investigated a general strategy that is based on the one-step electrospinning method to grow $CsPbX_3$ NC *in situ* in fibers.[19] The composition of $CsPbX_3$ can be finely tuned to be uniformly encapsulated in polymer (PS) fibers by reasonably adjusting the ratio of PbX_2 and CsX salts in the precursor solution. Fig. 7b displays a typical SEM image of the $CsPbBr_3$@PS fiber film with 300 mg mL^{-1} PS; the average diameter of the fibers is 800 nm. The average size of $CsPbBr_3$ NCs encapsulated in fibers is about 20 nm (Fig. 7c). Fig. 7d shows a clear absorption peak at around 500 nm and a PL emission peak at 513 nm with an FWHM of 24 nm. The PLQY values of $CsPbBr_3$@PS remained above 70% of their original

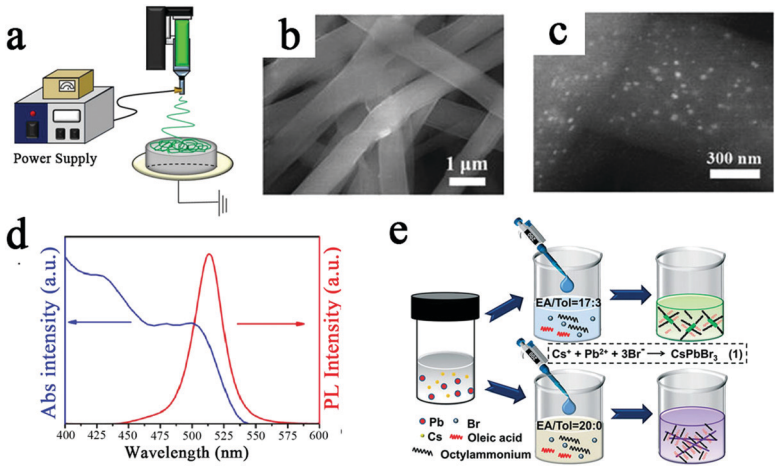

Fig. 7 (a) Schematic diagram of the $CsPbX_3$ (X = Cl, Br, I) nanofiber preparation process.[5] Copyright 2019, American Institute of Physics. (b) SEM images of the $CsPbBr_3$@PS fibers.[19] (c) Typical backscattered electron SEM images of the $CsPbBr_3$@PS fibers.[19] (d) UV-vis absorption and PL spectra of the $CsPbBr_3$@PS fibers.[19] Copyright 2018, John Wiley and Sons Inc. (e) Schematic diagram of the process for synthesising $CsPbBr_3$ nanorods and nanowires.[29] Copyright 2021, Royal Society of Chemistry.

values after immersion in water for 192 h and above 50% after heating at 80 °C for 120 min. Eventually, the $CsPbBr_3$@polymer fibers prepared by this method showed greatly improved water thermal stability and a PLQY of 48%.

Ligand-assisted reprecipitation (LARP) is also a facile method for the synthesis of $CsPbX_3$ NCs at room temperature. Lai *et al.* applied the green solvent acetic acid instead of DMF to the LARP technique for the controlled synthesis of $CsPbBr_3$ NCs under ambient conditions.[29] The workflow of LARP technology is shown in Fig. 7e. The length of the $CsPbBr_3$ NCs can be varied by changing the EA/Tol volume ratio to adjust the polarity of the antisolvent medium, enabling continuous conversion from nanorods to NWs. The prepared $CsPbBr_3$ NCs have broad photoluminescence (471–508 nm) and a high quantum yield of up to 78%.

To clearly summarize the preparation processes and optical properties of different $CsPbX_3$ materials, the recent

Table 1 Comparison of the optical properties of $CsPbX_3$ perovskite nanocrystals with different preparation methods

Materials	Shapes	Preparation methods	PL peaks (nm)	PLQY	FWHMs (nm)	Ref.
$CsPbBr_3$	Single crystal	Solution growth	530	—	17	18
$CsPbBr_3$	Single crystal	Bridgman growth	527–538	—	—	6
$CsPbBr_3$	Film	solution process	520	—	—	26
$CsPbBr_3$	Film	Thermal evaporation	522.5	15.7%	18.5	58
$CsPbBr_3$	Film	Thermal evaporation	525	12.2%	18	59
$CsPbBr_3$	Film	Thermal evaporation	547	—	—	16
$CsPbBr_3$	Film	Thermal evaporation	524	7.3%	18	62
$CsPbCl_3$	Film	Thermal evaporation	410	—	—	64
$CsPbX_3$	Film	Thermal evaporation	413.33–700.56	—	12.42–31.03	63
$CsPbX_3$	Nanocrystals	Hot injection	410–700	50–90%	12–42	17
$CsPbBr_3$	Nanocrystals	Hot injection	517	81% (in *n*-hexane)	17	7
$CsPbBr_{0.6}I_{2.4}$	Nanocrystals	Hot injection	653	85% (in *n*-hexane)	35	7
$CsPbBr_3$/MOF-5	Nanocrystals	Hot injection	519	52%	21	7
$CsPbBr_{0.6}I_{2.4}$/MOF-5	Nanocrystals	Hot injection	655	56%	35	7
$CsPbBr_3$/ZIF-8	Nanocrystals	Hot injection	520	72%	18	25
$CsPbCl_3$	Nanocrystals	Hot injection	408	65%	11	28
$CsPbBr_3$	Nanocrystals	Hot injection	512	92%	18	28
$CsPbI_3$	Nanocrystals	Hot injection	691	58%	32	28
$CsPbX_3$@zeolite	Nanocrystals	Hot injection	436–648	—	15.9–42	57
$CsPbBr_3$@SBS	Nanofiber	Electrospinning	513	29%	21	5
$CsPbBr_3$@PMMA	Nanofiber	Electrospinning	515	27%	22	5
$CsPbBr_3$@PS	Nanofiber	Electrospinning	516	23%	23	5
$CsPbX_3$	Nanocrystals	Electrospinning	450–660	—	18–35	46
$CsPbX_3$	Nanofiber	Electrospinning	405–675	—	16–35	65
$CsPbBr_3$	Nanofiber	Electrospinning	517	—	—	66
CNTs/$CsPbBr_3$@PAN	Nanofiber	Electrospinning	511	—	20	67
$CsPbBr_3$@PS	Fiber	Electrospinning	517	45.7%	—	68
$CsPbBr_3$@PS	Fiber	Electrospinning	518	37%	22	70
$CsPbBr_3$	Nanofiber	Electrospinning	521.26	—	20.19	70
$CsPbBr_3$	Nanocrystals	LARP	471–508	78%	—	29
$CsPbBr_3$	Nanocrystals	LARP	507	82.2%	26	81

developments of the different preparation methods and different compositions of $CsPbX_3$ are detailed in Table 1.

3. Applications of $CsPbX_3$ perovskites

3.1 Perovskite solar cells

OIH perovskites have been studied for decades and have received increasing attention in recent years for their application prospects in the photovoltaic field due to their excellent photovoltaic properties.[77] However, compared to OIH perovskites, all-inorganic perovskites have better thermal stability. Therefore, the application of all-inorganic chalcogenides in solar cells can yield excellent wet thermal stability.[44,78] Next, the application of all-inorganic $CsPbX_3$ perovskites in the field of solar cells will be presented.

Some scholars have incorporated organic molecules into $CsPbX_3$ PSCs to achieve efficient and stable inorganic $CsPbX_3$ PSCs.[79] Recently, Zhou *et al.* incorporated inorganic 2D Cl-terminated Ti_3C_2 ($Ti_3C_2Cl_x$) MXene into $CsPbBr_3$ films; the all-inorganic $CsPbBr_3$ PSC showed an efficiency of 11.08% and an open-circuit voltage of up to 1.702 V, which is the highest recorded in $CsPbBr_3$ solar cells.[80] Shao *et al.* obtained Cs-rich $FA_{0.15}Cs_{0.85}PbI_3$ perovskite by doping FA cations into $CsPbI_3$ perovskite, which improved its thermal and moisture stability.[4] The $FA_{0.15}Cs_{0.85}PbI_3$ films were used as the active layer to prepare solar cells with FTO/compact-TiO_2/mesoporous-TiO_2/perovskite/Spiro-OMeTAD/Au. As shown in Fig. 8a, the *J–V* curve demonstrated a V_{OC} of 1.02 V, J_{SC} of 21.4 mA cm^2, and fill factor of 80.0%. The external quantum efficiency (EQE) of the $FA_{0.15}Cs_{0.85}PbI_3$ solar cell is displayed in Fig. 8b. The $FA_{0.15}C_{s0.85}PbI_3$ perovskite solar cell achieved a high PCE of 17.5%.

In the second section of this paper, the preparation of $CsPbX_3$ perovskite by thermal evaporation is presented, and the solution-processed devices in the field of photovoltaics usually are significantly better than those fabricated by thermal

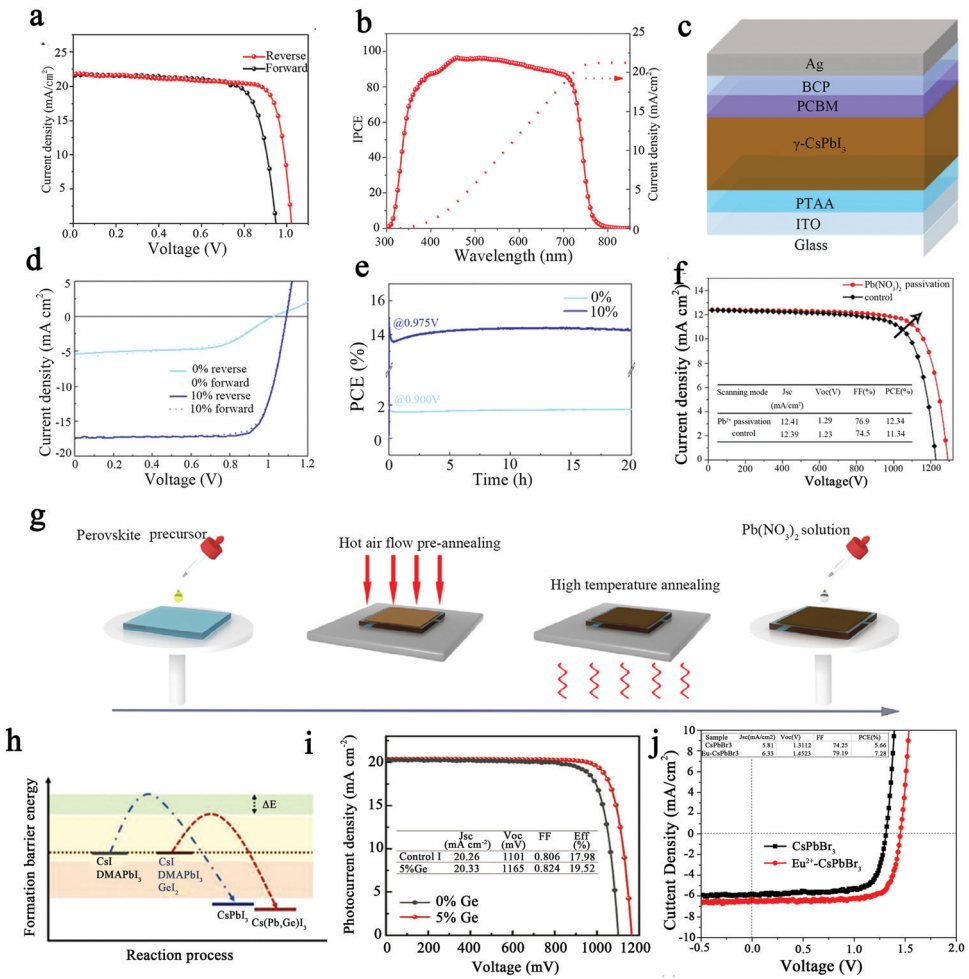

Fig. 8 (a) *J–V* curve of $FA_{0.15}Cs_{0.85}PbI_3$ solar cells.[4] (b) EQE curves of $FA_{0.15}Cs_{0.85}PbI_3$ solar cells.[4] Copyright 2020, Wiley-Blackwell. (c) Structure of a $CsPbI_3$ perovskite solar cell.[21] (d) *J–V* characteristics of $CsPbI_3$ (0%) and $CsPbI_3$ with a 10% PEAI device.[21] (e) PCE of $CsPbI_3$ (0%) and $CsPbI_3$ with a 10% PEAI device.[21] Copyright 2021, Wiley-VCH Verlag. (f) *J–V* curves for the passivated $CsPbI_2Br$ devices and control devices.[32] (g) Schematic diagram of the fabrication of perovskite films and the passivation process using $Pb(NO_3)_2$ ethyl acetate solution.[32] Copyright 2018, Wiley-Blackwell. (h) Schematic diagram of the crystallization kinetics of $CsPbI_3$ and Ge-doped $CsPbI_3$ thin films.[38] (i) *J–V* curves of the champion $CsPb_{0.95}Ge_{0.05}I_3$-based PSC and control group.[38] Copyright 2021, Wiley-VCH Verlag. (j) *J–V* curves of $CsPbBr_3$ and Eu^{2+}-doped $CsPbBr_3$-based PSC.[42] Copyright 2020, Wiley-Blackwell.

evaporation. Nevertheless, Zhang *et al.* prepared high-quality γ-$CsPbI_3$ perovskite layers with PCEs of up to 15% by thermal evaporation of PbI_2 and CsI with a small amount of phenylethylammonium iodide (PEAI), exceeding the performance of most solution-processed inorganic $CsPbX_3$ (X = Cl, Br, I) PEAI perovskite solar cells.[21] Fig. 8c shows the structure of the $CsPbI_3$ solar cell. The addition of the appropriate amount of PEAI not only provided high-quality perovskite films but also ensured charge transport in the active layer of the perovskite films, which exhibited a longer charge recombination lifetime; this indicates that the charge recombination is strongly suppressed, thus improving the performance of the PSCs. Fig. 8d displays the current density–voltage (*J*–*V*) characteristics of the device with a V_{OC} of 1.09 V, J_{SC} of 17.33 mA cm^2, and fill factor of 79.41%. When PEAI was added at 10%, the device obtained 15% PCE, as shown in Fig. 8e.

Traps on the surface of perovskite can affect the conversion efficiency of perovskite solar cells. In recent years, some scholars have used post-treatment methods to reduce surface traps to further improve the PCE of inorganic PSCs. Yuan *et al.* introduced a Pb^{2+} solution post-processing strategy to passivate the deep trap state of $CsPbI_2Br$ films and obtained PSCs with a PCE of 12.34%.[32] The dissociative Pb^{2+} in the solution can combine with the excess halide ions on the surface of perovskite, thus reducing the deep trap density of states and charge recombination. The reduction of defect states results in doubling of the average lifetime of perovskite, increasing the V_{OC} and PCE of the solar cell device. The preparation and passivation process of $CsPbI_2Br$ perovskite films is shown in Fig. 8g. The structure of the planar heterojunction perovskite solar cells is in the form of FTO/SnO_2/perovskite/spiro-OMeTAD/Ag. SnO_2 is used as an electron transport layer to reduce the hysteresis effect, resulting in a J_{SC} of 12.41 mA cm^2, V_{OC} of 1.29 V, and FF of 76.9% for perovskite solar cells, as shown in Fig. 8f. In addition, Li *et al.* synthesized *n*-methyl-2-pyrrolidinone iodide (NMPI) as a functional precursor additive to improve the phase stability and optical properties of $CsPbI_3$.[82] As a result, the PCE of the quasi-2D (n = 20) $CsPbI_3$ PSC was increased to 14.59%, and the stability was significantly enhanced.

Doping has been used to participate in the crystallization process, altering the energy state of the perovskite and promoting the stability of the PSCs. Meng *et al.* found that Ge doping was able to modify the crystalline growth of $CsPb_{1-x}Ge_xI_3$ films and reduce the annealing temperature and processing time by lowering the $CsPbI_3$ formation energy.[38] As shown in Fig. 8h, the first addition of Ge to the precursor of $DMAPbI_3$ accelerated the crystallization process by lowering the formation energy and improving the thermodynamic stability. The GeO_2 generated in situ on the surface of the perovskite film acts as a passivation layer to passivate the grain boundaries and surface defects, thereby improving the hygrothermal stability of the perovskite film and PSCs. The device structure of the solar cell is FTO/compact TiO_2(c-TiO_2)/PCBA/perovskite/spiro-OMeTAD/Au. As shown in Fig. 8i, the PCE of the best PSC is 19.52% (a certified PCE of 18.8%) with a J_{SC} of 20.33 mA cm^{-2}, V_{OC} of 1165 mV, and FF of 0.824. Karunakaran *et al.* doped Eu^{2+} into all-inorganic $CsPbBr_3$ PSCs, leading to an increase in PCE from 5.66% to 7.28%.[42] Owing to the addition of rare earth elements, the perovskite films displayed crystallinity and smooth morphology while optimizing the charge transfer kinetics within the perovskite films. As shown in Fig. 8j, the photovoltaic performance was greatly improved when Eu^{2+} was introduced up to 60 μL.

This section focuses on the enhancement of the performance of all-inorganic PSCs by doping, which passivates the surface defects of perovskite and improves the average lifetime, thus optimizing the performance of PSCs. At the end of this section, some of the advances in $CsPbX_3$ perovskite solar cells reported in the literature are summarized in Table 2.

3.2 Light-emitting diodes

Recently, increasing numbers of scholars have applied all-inorganic perovskite as light-emitting materials in LEDs. Next, we describe the application of perovskite with different luminescent colors in LEDs. The PN junctions are the basis for LEDs, where electrons and holes will migrate directionally and recombine near the PN junction when a forward bias is applied, releasing heat or light.[88] Tang *et al.* prepared $CsPbBr_3$ green-emitting LEDs by all-vacuum processing, and high-throughput combination strategies were adopted to optimize the perovskite composition, annealing temperature and functional layer thickness.[8] The structure of $CsPbBr_3$ perovskite LED is indium-doped tin oxide (ITO)/LiF/perovskite/TPBi/LiF/Al, and the energy band diagram of the AVBD-processed device is shown in Fig. 8a. When the Cs/Pb ratio and the thickness of the perovskite film are 1.17 : 1 and 110.6 nm, the LED will achieve optimal performance. The appropriate functional layer thickness can balance electron and hole injection, thus enhancing the EQE of the LED performance. The best device showed a current efficiency (CE) of 4.8 cd A^{-1} (EQE of 1.45%) at 2358 cd m^{-2}, as shown in Fig. 9a. In addition, the CE improved to 10.15 cd A^{-1} and the EQE improved to 3.26% for perovskite LEDs by improving the hole-injection layer to NiO_x. $CsPbX_3$ perovskite is usually prepared in an inert environment under high temperature conditions, which hinders the large-scale production of LED devices, and a low-temperature preparation strategy is essential. Wang *et al.* synthesized $CsPbBr_3$ NCs in the

Table 2 Performance comparison of the PSCs based on $CsPbX_3$ perovskites

Materials	J_{SC} (mA cm^2)	V_{OC} (V)	FF (%)	PCE (%)	Ref.
$FA_{0.15}Cs_{0.85}PbI_3$	21.4	1.02	80	17.5	4
$CsPbX_3$	17.33	1.09	79.41	15	21
$CsPbI_2Br$	12.41	1.29	76.90	12.34	32
$CsPbX_3$	12.6	1.05	78.70	10.40	83
$CsPbI_3$	15.68	1.20	64	12.04	84
$CsPbI_2Br$	15.34	1.32	80	16.14	85
$CsPbI_2Br$	15.23	1.14	64.51	11.20	86
$CsPbI_3$	0.415	0.643	42.9	0.11	87
$CsPbBr_3$	2.96	0.851	44.5	1.21	87
$CsPb_{1-x}Ge_xI_3$	20.33	1.165	82.4	18.8	38
$CsPbBr_3$	6.33	1.4523	79.19	7.28	42

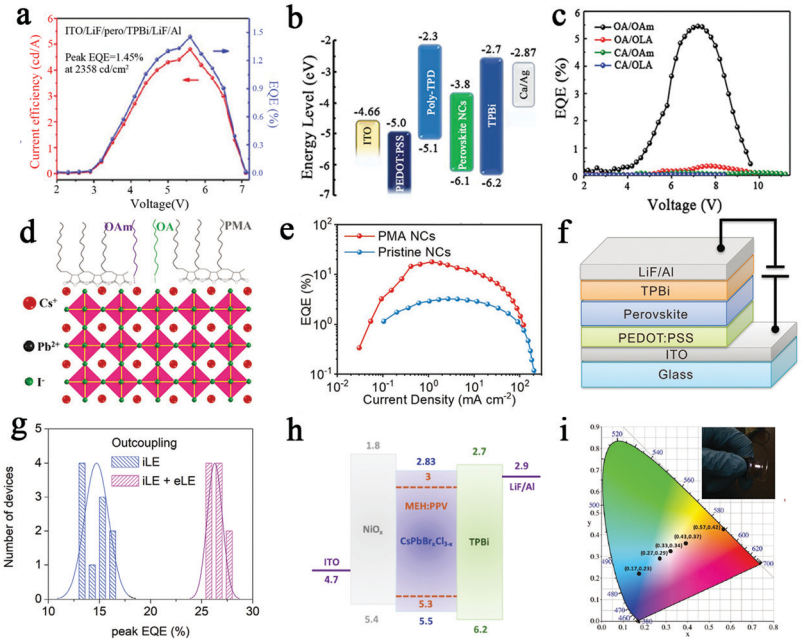

Fig. 9 (a) Current efficiency and EQE curves of the best device.[8] Copyright 2019, Wiley-VCH Verlag. (b) Energy level diagram of LED devices.[20] (c) External quantum efficiency *versus* voltage of LED devices.[20] Copyright 2019, Wiley-Blackwell. (d) Schematic diagram of the PMA-incorporating β-$CsPbI_3$ NCs.[27] (e) Relationship between the current density and EQE curve of the $CsPbI_3$ LED.[27] Copyright 2020, Wiley-Blackwell. (f) Schematic diagram of the structure of the PSC devices.[33] (g) Histogram of the EQEs of the devices.[33] Copyright 2021, Wiley-VCH Verlag. (h) Schematic of the band structure.[39] (i) CIE coordinates of the white LED.[39] Copyright 2016, Wiley-Blackwell.

presence of the short-chain ligands propionic acid (PA) and butylamine (BLA) in a room temperature environment.[20] In addition, studies have shown that $CsPbBr_3$ NCs anchored by OA and OAm produce the best performance. Fig. 9b shows the energy level diagram of the $CsPbBr_3$ LED and the structural composition of each part of the device. Fig. 9c demonstrates that the LEDs with OA/OAm-anchored NCs exhibit the best performance over a wide range, with a luminance of 5033 Cd m^{-2}, CE of 18.6 Cd A^{-1}, turn-on voltage as low as 3.2 V, and EQE of 5.4%.

The stability of perovskite LEDs has been a great challenge, especially as red perovskite LEDs typically have a lifetime of only a few hours. Li *et al.* have prepared stable β-$CsPbI_3$ for red-emitting LED applications through incorporation of poly(maleicanhydride-*alt*-1-octadecene) (PMA) in synthesizing the nanocrystals.[27] As shown in Fig. 9d, the PMA can interact with PbI_2 in the precursor through the coupling between the O group in PMA and Pb^{2+}, and the PMA greatly passivated Pb_{Cs} anti-situ defects on the surface of β-$CsPbI_3$, which improved the stability of the crystal. The photoluminescence quantum yield of the β-$CsPbI_3$ NCs films was significantly increased from 34% to 89% due to the addition of PMA. The structure of this device is indium tin oxide (ITO)/poly(3,4-ethylenedioxythiophene) polystyrene sulfonate (PEDOT:PSS)/poly-TPD/β-CsPbI3 NCs/tris(1-phenyl-1*H*-benzimidazole) (TPBi)/lithium fluoride (LiF)/Al. Fig. 9e shows red-emitting LEDs obtaining an EQE of 17.8%. The LEDs were stable for 317 h at a constant current density of 30 mA cm^{-2}. Miao *et al.* prepared γ-$CsPbI_3$ cuboid crystallites of deep red light perovskite LEDs based on a one-step method.[89] Due to the addition of diammonium iodide to passivate the trap state of the *in situ* formed γ-$CsPbI_3$, the high peak external quantum efficiency (EQE) value of the LED was 15.03%. Moreover, this one-step method offers a new strategy for the flow-line production of large-area perovskite LED modules.

Most of the current research on perovskite blue-emitting LEDs has been prepared by adjusting the band gap of a mixture of Br and I halogens. However, the film morphology of the mixed halide perovskite has not been well improved. Yao *et al.* prepared blue-emitting (470 nm) perovskite nanocrystals by mixing a 2 : 1 weight ratio of $CsPbBr_3$ and $CsPbI_3$ nanocrystals.[39] By controlling the size of the thin film grains, high quality blue-emitting perovskite LEDs were obtained. Shen *et al.* proposed a simple device architecture to achieve highly efficient blue-emitting perovskite LEDs.[33] Interfacial engineering is employed to manipulate the perovskite crystallization to achieve highly compact perovskite nanocrystals. The device structure of the blue perovskite LEDs is shown in Fig. 9f. On this basis, the EQE is further increased from 16.8% to 27.5% by integrating a lens-based structure for substrate mode light (Fig. 9g).

The preparation process of white perovskite LEDs is more complex than that of red, blue and green LEDs. Yao *et al.*, mentioned in the previous paragraph, prepared a white light perovskite LED by mixing an orange light polymer with blue perovskite as the active layer.[39] The device structure of white LEDs with a composite orange polymer material is shown in Fig. 9h. By adjusting the ratio between perovskite nanocrystals and polymers, white LEDs were achieved with CIE coordinates at (0.33, 0.34). Chen *et al.* first prepared red-emitting $CsPbBr_{2.5}I_{0.5}$ perovskite films by a one-step spin-coating method using polyacrylonitrile

(PAN) polymer.[90] Then, white LEDs were prepared by combining *N*,*N*′-bis(naphthalen-1-yl)-*N*,*N*′-bis(phenyl)-benzidine (NPB), $CsPbBr_{2.5}I_{0.5}$ perovskite films doped with PAN, and $CsPbBr_3$. As shown in Fig. 9i, the LEDs displayed a maximum of 360 cd m^{-2} with CIE coordinates of (0.31, 0.36) at 7 V.

For further study, some optical parameters of $CsPbX_3$ perovskite-based LEDs are summarized in Table 3. In recent years, many different methods of preparing perovskite LEDs have emerged, gradually improving their luminescence properties and stability. All-inorganic perovskite LEDs show great promise in the field of optical displays.

3.3 Photodetectors

$CsPbX_3$ perovskite is used in photodetectors due to its high light absorbance and long carrier diffusion length. Next, we describe the application of different structures of perovskite in photodetectors. Zeng *et al.* prepared $CsPbBr_3$ nanosheets by improving the hot injection method and applied them in photodetectors.[3] As shown in Fig. 10a, the edge length of the nanosheet could be greater than 1.5 μm. Large-area $CsPbBr_3$ nanosheet films were prepared by simple ink printing or the roll-to-roll method and applied to flexible photodetectors, as shown in Fig. 10b. In the presence of an external electric field, the electron-hole pairs generated in the perovskite are rapidly separated and collected by the copper electrode, and then the $CsPbBr_3$ nanosheet photodetector can work effectively. As shown in Fig. 10c, the maximum value of the responsivity was located at 517 nm, and the responsivity was 0.64 A W^{-1}; the peak EQE value of the device at 515 nm was 53% at 10 V bias. A visible photodetector prepared using $CsPbBr_3$ nanosheets exhibited a high sensitivity with a light on/off ratio of $>10^3$ under 442 nm light at a power of 0.35 mW cm^{-2} as well as high stability and outstanding fluorescence excitability ($>10\,000$ cycles). In addition, high stability and outstanding fluorescence excitability were still demonstrated after 10 000 cycles.

Large perovskite single crystals have the potential to produce high performance photodetectors due to their higher carrier mobility, longer diffusion length and longer carrier lifetime. Zheng *et al.* demonstrated a low-temperature and substrate-independent strategy to prepare millimeter-scale $CsPbBr_3$ perovskite single-crystal films.[23] Fig. 10d shows a schematic of the device structure. The superior carrier transport properties will improve the performance of the photodetector. The trap density, diffusion length and migration lifetime of $CsPbBr_3$ films and $CsPbBr_3$ bulk crystals are comparable, but the resistivity is superior to that of the $CsPbBr_3$ bulk crystals, which improves the performance of the photodetector. Fig. 10e shows the photodetector with a light on/off ratio $>10^3$ and rise and decay times of 0.4 ms and 9 ms, respectively. The $CsPbBr_3$ films showed no significant photoluminescence loss after two months of storage, indicating that they exhibited excellent long-term stability to humidity and heat treatment. Ramasamy *et al.* prepared $CsPbX_3$ (X = Cl, Br, I) nanocrystals (NCs) using halide ion exchange reactions at room temperature, and the photoluminescence could be tuned throughout the visible region (425–655 nm).[31] In this report, $CsPbBr_3$ perovskite colloidal NCs prepared by halogen exchange reactions were applied to photodetectors for the first time. An adjustable luminescence range was achieved through the halide ion exchange reactions. The green emission from $CsPbBr_3$ NCs was tuned by lithium salts (LiX, X = I, Cl, Br) in the entire visible spectral region (425–655 nm) at room temperature. Fig. 10f demonstrates that different concentrations of lithium salts can tune the PL peak from 508 to 654 nm. The group selected $CsPbI_3$ NCs with relatively long radiation lifetimes for photodetector applications. The $CsPbI_3$ photodetector exhibits an excellent on/off photocurrent ratio of 10^5. In addition, the $CsPbI_3$ photodetector showed a relatively fast rise time (t_{rise} = 24 ms) and decay time (t_{decay} = 29 ms), as shown in Fig. 10g.

Planar heterojunction (PHJ) structures consisting of different semiconductors also show great potential in photodetectors. Chen *et al.* prepared solution-processed perovskite quantum dots (PQDs)/organic semiconductors (OSC) planar heterojunctions and applied them to photodetectors.[37] $CsPbBr_3$ QDs were prepared by the hot-injection method, and the quantum dot films were prepared by spin coating. Fig. 10h shows a schematic of the phototransistor for $CsPbBr_3$

Table 3 Performance comparison of the LEDs based on $CsPbX_3$ perovskites

Materials	Luminous colours	EL λ_{max} (nm)	V_{on} (V)	Max. EQE (%)	Max. CE (cd A^{-1})	Max. L (cd m^{-2})	Ref.
$CsPbBr_3$	Green	523–524	3.92	—	1.07	1607	62
$CsPbBr_3$	Green	516	—	1.45	4.8	2358	8
$CsPbBr_3$	Green	516	3.2	5.4	18.6	5033	20
$CsPbBr_3$	Green	514	—	13.14	37.14	45 990	26
$CsPbBr_3$	Green	517	2.3	5.7	19.9	46 000	91
$CsPbBr_3$	Green	516	4.2	0.12	0.43	946	50
$CsPbI_3$	Green	586	4.6	0.09	0.08	528	50
$CsPbCl_3$	Green	455	5.1	0.07	0.14	742	50
$CsPbBr_3$	Green	—	—	0.25	0.96	637	92
$CsPbBr_3$	Green	510	2–2.5	0.37	0.72	1661	93
$CsPbI_3$	Red	689	5	17.8	—	618	27
$CsPbI_3$	Red	699	2.8	15.3	—	1272	89
$CsPbBr_xCl_{3-x}$	Blue	470	5	0.07	0.18	350	39
$CsPbBr_{3-x}Cl_x$	Blue	486	3.3	27.5	33.4	3651	33
$CsPb(Br_{2.5}I_{0.5})$ + $CsPbBr_3$	White	—	7	—	0.2	360	90
$CsPbBr_xCl_{3-x}$ + MEH:PPV	White	—	8	—	—	—	39

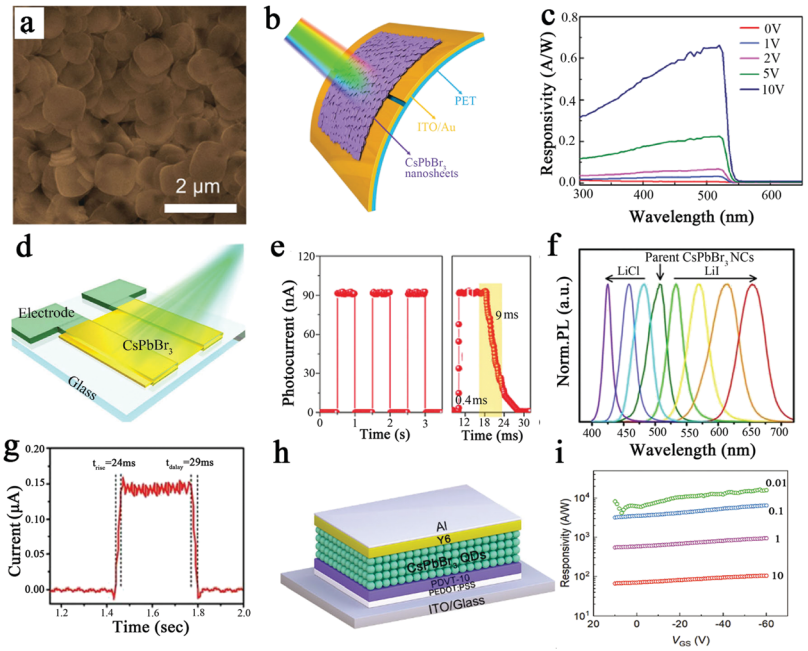

Fig. 10 (a) SEM images of $CsPbBr_3$ nanosheets.[3] (b) Schematic diagram of PDs based on $CsPbBr_3$ nanosheets.[3] (c) Responsivity of $CsPbBr_3$ nanosheet photodetector devices under different forward biases.[3] Copyright 2016, Wiley-Blackwell. (d) Schematic of the photodetector device structure.[23] (e) Left: Time-dependent optical response of the photoelectric detector. Right: Rise time and decay time of the photodetector under 530 nm light (216 μW m^{-2}) at a bias of 2 V.[23] Copyright 2018, Wiley-Blackwell. (f) PL spectra of $CsPbBr_3$ NCs exchanged with different concentrations of LiI and LiCl.[31] (g) Rise and decay times of the photodetector device.[31] Copyright 2016, Royal Society of Chemistry. (h) Schematic device structure of the $CsPbBr_3$ QDs/PDVT-10 phototransistor.[37] (i) Responsivity of $CsPbBr_3$ QDs/PDVT-10 phototransistors.[37] Copyright 2021, Wiley-VCH Verlag.

QDs/PDVT-10 PHJs. As shown in Fig. 10i, the *R*-value can reach 1.64×10^4 A W^{-1} when the illumination intensity is 0.01 mW cm^{-2}. In addition, the double layer PQD/PDVT-10 PHJs phototransistor has a specific detectivity of 3.17×10^{12} Jones and a photosensitivity of 5.33×10^6. The presence of the PHJ structure allows the exciton dissociation process to become more efficient. This photosensitive effect is important for achieving high responsiveness or gain in PHJ-based phototransistors due to the extended excess carrier lifetime. For comparison, the properties of $CsPbX_3$ perovskite PDs are summarized in Table 4.

4. Conclusions

In summary, here, we reviewed some advances in OIH perovskites, mainly some different preparation methods of all-inorganic perovskites and their applications in optoelectronic fields. Recently, due to the special physical structure and excellent optical properties of $CsPbX_3$ perovskite, researchers have conducted extensive research on $CsPbX_3$. However, there are still some challenges in the practical application of perovskite remaining to be addressed. Therefore, in this section, we focus on a summary of the current challenges and opportunities for perovskite applications.

Firstly, the toxicity of lead halide perovskite needs to be considered. The heavy metal ion lead has severe consequences on human health and the environment. Appropriate encapsulation strategies are needed to reduce the toxicity of lead halide perovskite. When the lead halide perovskite encapsulated by the polymer is exposed to water, the lead concentration is comparable to that in tap water. Another alternative solution is the development of lead-free halide perovskite, a non-toxic element (such as Sn, Bi, Sb, Cu, and Ge) to replace the toxic lead.[94]

Secondly, the instability of the internal structure of perovskite is also a problem that limits its commercialization. The water stability of perovskite has been improved through different approaches, including surface passivation and the polymer encapsulation strategy. However, polymer encapsulation can affect the electrical properties of perovskites, reducing

Table 4 Performance comparison of photodetectors based on $CsPbX_3$ perovskites

Materials	Shapes	Responsivity (A W^{-1})	On/off ratio	Rise time (ms)	Decay time (ms)	EQE (%)	Ref.
$CsPbBr_3$	Nanosheet	0.64	$>10^4$	0.019	0.24	54	3
$CsPbBr_3$–CNTs	Nanosheet	31.1	>832	0.016	0.38	—	95
$CsPbBr_3$	Film	0.21	10^3	0.4	9	6.2	23
$CsPbBr_3$/ZnO	Film	4.25	$>10^4$	0.21	0.24	—	96
$CsPbI_3$	Nanocrystal	—	10^5	24	29	—	31

the efficiency of their optoelectronic devices. Subsequent research needs to focus on surface modification, improvement of surface passivation strategies or improvement of chemical components.

Third, compared to OIH perovskites, the band gap of all-inorganic perovskites should be suitably adjusted to better improve the performance of optoelectronic devices. Therefore, the band gap of all-inorganic perovskites is tuned and their stability is further improved by doping, metal-organic framework crystal embedding and ligand-based studies.

Ultimately, we hope that theoretical calculations and experiment studies in $CsPbX_3$ will be of great benefit to the synthesis of crystals and device performance. All-inorganic perovskites still have a long way to go, but we believe that they will make great progress in a variety of applications. $CsPbX_3$ can play important roles in photovoltaics and improving human well-being.

Conflicts of interest

There are no conflicts to declare.

Acknowledgements

This work was supported by the National Science Foundation of China (No. 61904123), the Natural Science Foundation of Tianjin (No. 18JCQNJC71800), Scientific Research Project of Tianjin Educational Committee (No. 2018KJ220), Tianjin Technical and Engineering Center of Nonwovens (No. KF202103).

Notes and references

1 M. Z. Liu, M. B. Johnston and H. J. Snaith, Efficient planar heterojunction perovskite solar cells by vapour deposition, *Nature*, 2013, **501**(7467), 395–398.

2 J. Shamsi, A. S. Urban, M. Imran, L. De Trizio and L. Manna, Metal Halide Perovskite Nanocrystals: Synthesis, Post-Synthesis Modifications, and Their Optical Properties, *Chem. Rev.*, 2019, **119**(5), 3296–3348.

3 J. Z. Song, L. M. Xu, J. H. Li, J. Xue, Y. H. Dong, X. M. Li and H. B. Zeng, Monolayer and Few-Layer All-Inorganic Perovskites as a New Family of Two-Dimensional Semiconductors for Printable Optoelectronic Devices, *Adv. Mater.*, 2016, **28**(24), 4861–4869.

4 Z. P. Shao, H. G. Meng, X. F. Du, X. H. Sun, P. L. Lv, C. Y. Gao, Y. Rao, C. Chen, Z. P. Li, X. Wang, G. L. Cui and S. P. Pang, Cs_4PbI_6-Mediated Synthesis of Thermodynamically Stable $FA_{(0.15)}Cs_{(0.85)}PbI_{(3)}$Perovskite Solar Cells, *Adv. Mater.*, 2020, **32**(30), DOI: **10.1002/adma.202001054**.

5 D. H. Jiang, Y. H. Tsai, L. Veeramuthu, F. C. Liang, L. C. Chen, C. C. Lin, T. Satoh, S. H. Tung and C. C. Kuo, Novel ultra-stable and highly luminescent white light-emitting diodes from perovskite quantum dots-Polymer nanofibers through biaxial electrospinning, *Appl. Mater.*, 2019, 7(11), DOI: **10.1063/1.5124880**.

6 J. Z. Song, Q. Z. Cui, J. H. Li, J. Y. Xu, Y. Wang, L. M. Xu, J. Xue, Y. H. Dong, T. Tian, H. D. Sun and H. B. Zeng, Ultralarge All-Inorganic Perovskite Bulk Single Crystal for High-Performance Visible-Infrared Dual-Modal Photodetectors, *Adv. Opt. Mater.*, 2017, **5**(12), DOI: **10.1002/adom.201700157**.

7 J. J. Ren, T. R. Li, X. P. Zhou, X. Dong, A. V. Shorokhov, M. B. Semenov, V. D. Krevchik and Y. H. Wang, Encapsulating all-inorganic perovskite quantum dots into mesoporous metal organic frameworks with significantly enhanced stability for optoelectronic applications, *Chem. Eng. J.*, 2019, **358**, 30–39.

8 J. H. Li, P. P. Du, S. R. Li, J. Liu, M. H. Zhu, Z. F. Tan, M. C. Hu, J. J. Luo, D. Q. A. Guo, L. Ma, Z. G. Nie, Y. Ma, L. Gao, G. D. Niu and J. Tang, High-Throughput Combinatorial Optimizations of Perovskite Light-Emitting Diodes Based on All-Vacuum Deposition, *Adv. Funct. Mater.*, 2019, **29**(51), DOI: **10.1002/adfm.201903607**.

9 N. Lakhdar and A. Hima, Electron transport material effect on performance of perovskite solar cells based on $CH_3NH_3GeI_3$., *Opt. Mater.*, 2020, 99.

10 J. Y. Guan, J. Ni, X. J. Zhou, Y. Liu, J. Y. Yin, J. L. Wang, D. Wang, Y. F. Zhang, J. Li, H. K. Cai and J. J. Zhang, High-Performance Electron Transport Layer via Ultrasonic Spray Deposition for Commercialized Perovskite Solar Cells, *ACS Appl. Energy Mater.*, 2020, **3**(12), 11570–11580.

11 H. Sung, N. Ahn, M. S. Jang, J. K. Lee, H. Yoon, N. G. Park and M. Choi, Transparent Conductive Oxide-Free Graphene-Based Perovskite Solar Cells with over 17% Efficiency, *Adv. Energy Mater.*, 2016, **6**(3), DOI: **10.1002/aenm.201501873**.

12 J. H. Heo and S. H. Im, $CH_3NH_3PbBr_3$–$CH_3NH_3PbI_3$ Perovskite-Perovskite Tandem Solar Cells with Exceeding 2.2 V Open Circuit Voltage, *Adv. Mater.*, 2016, **28**(25), 5121–5125.

13 M. A. Green, A. Ho-Baillie and H. J. Snaith, The emergence of perovskite solar cells, *Nat. Photonics*, 2014, **8**(7), 506–514.

14 H. Tang, S. S. He and C. W. Peng, A Short Progress Report on High-Efficiency Perovskite Solar Cells, *Nanoscale Res. Lett.*, 2017, 12.

15 G. A. Al-Dainy, S. E. Bourdo, V. Saini, B. C. Berry and A. S. Biris, Hybrid Perovskite Photovoltaic Devices: Properties, Architecture, and Fabrication Methods, *Energy Technology*, 2017, **5**(3), 373–401.

16 J. Lei, F. Gao, H. X. Wang, J. Li, J. X. Jiang, X. Wu, R. R. Gao, Z. Yang and S. Z. Liu, Efficient planar $CsPbBr_3$ perovskite solar cells by dual-source vacuum evaporation, *Solar Energy Mater. Solar Cells*, 2018, **187**, 1–8.

17 L. Protesescu; S. Yakunin; M. I. Bodnarchuk; F. Krieg; R. Caputo; C. H. Hendon; R. X. Yang; A. Walsh and M. V. Kovalenko, Nanocrystals of Cesium Lead Halide Perovskites ($CsPbX_3$, X = Cl, Br, and I): Novel Optoelectronic Materials Showing Bright Emission with Wide Color Gamut. *Nano Lett.* 2015, 15 (6), 3692–3696.

18 Y. P. Fu, H. M. Zhu, C. C. Stoumpos, Q. Ding, J. Wang, M. G. Kanatzidis, X. Y. Zhu and S. Jin, Broad Wavelength Tunable Robust Lasing from Single-Crystal Nanowires of Cesium Lead Halide Perovskites ($CsPbX_3$, X = Cl, Br, I), *ACS Nano*, 2016, **10**(8), 7963–7972.

19 H. Liao, S. B. Guo, S. Cao, L. Wang, F. M. Gao, Z. B. Yang, J. J. Zheng and W. Y. Yang, A General Strategy for In Situ Growth of All-Inorganic $CsPbX_3$ (X = Br, I, and Cl) Perovskite Nanocrystals in Polymer Fibers toward Significantly Enhanced Water/Thermal Stabilities, *Adv. Opt. Mater.*, 2018, **6**(15), DOI: **10.1002/adom.201800346**.

20 F. H. Ye, H. J. Zhang, W. Li, Y. Yan, J. L. Cai, R. S. Gurney, A. J. Pearson, D. Liu and T. Wang, Ligand-Exchange of Low-Temperature Synthesized $CsPbBr_3$ Perovskite toward High-Efficiency Light-Emitting Diodes, *Small Methods*, 2019, **3**(3), DOI: **10.1002/smtd.201800489**.

21 Z. B. Zhang, R. Ji, M. Kroll, Y. J. Hofstetter, X. K. Jia, D. Becker-Koch, F. Paulus, M. Loffler, F. Nehm, K. Leo and Y. Vaynzof, Efficient Thermally Evaporated gamma-$CsPbI_3$ Perovskite Solar Cells, *Adv. Energy Mater.*, 2021, **11**(29), DOI: **10.1002/aenm.202100299**.

22 K. Wang, L. Y. Zheng, T. Zhu, X. Yao, C. Yi, X. T. Zhang, Y. Cao, L. Liu, W. P. Hu and X. Gong, Efficient perovskite solar cells by hybrid perovskites incorporated with heterovalent neodymium cations, *Nano Energy*, 2019, **61**, 352–360.

23 Z. Yang, Q. Xu, X. D. Wang, J. F. Lu, H. Wang, F. T. Li, L. Zhang, G. F. Hu and C. F. Pan, Large and Ultrastable All-Inorganic $CsPbBr_3$ Monocrystalline Films: Low-Temperature Growth and Application for High-Performance Photodetectors., *Adv. Mater.*, 2018, **30**(44), DOI: **10.1002/adma.201802110**.

24 J. Liang, J. Liu and Z. Jin, All-Inorganic Halide Perovskites for Optoelectronics: Progress and Prospects, *Solar Rrl*, 2017, **1**(10), DOI: **10.1002/solr.201700086**.

25 Y. B. Zhao, C. Xie, X. Zhang and P. Yang, $CsPbX_3$ Quantum Dots Embedded in Zeolitic Imidazolate Framework-8 Microparticles for Bright White Light-Emitting Devices, *ACS Appl. Nano Mater.*, 2021, **4**(5), 5478–5485.

26 L. P. Cheng, J. S. Huang, Y. Shen, G. P. Li, X. K. Liu, W. Li, Y. H. Wang, Y. Q. Li, Y. Jiang, F. Gao, C. S. Lee and J. X. Tang, Efficient $CsPbBr_3$ Perovskite Light-Emitting Diodes Enabled by Synergetic Morphology Control, *Adv. Opt. Mater.*, 2019, **7**(4), DOI: **10.1002/adom.201801534**.

27 H. M. Li, H. Lin, D. Ouyang, C. L. Yao, C. Li, J. Y. Sun, Y. L. Song, Y. F. Wang, Y. F. Yan, Y. Wang, Q. F. Dong and W. C. H. Choy, Efficient and Stable Red Perovskite Light-Emitting Diodes with Operational Stability >300 h, *Adv. Mater.*, 2021, **33**(15), DOI: **10.1002/adma.202008820**.

28 M. Imran, V. Caligiuri, M. J. Wang, L. Goldoni, M. Prato, R. Krahne, L. De Trizio and L. Manna, Benzoyl Halides as Alternative Precursors for the Colloidal Synthesis of Lead-Based Halide Perovskite Nanocrystals, *J. Am. Chem. Soc.*, 2018, **140**(7), 2656–2664.

29 W. W. Lai, C. L. Wu, W. H. Li and X. X. Han, Green solvent assisted preparation of one-dimensional $CsPbBr_3$ nanocrystals with a controllable morphology for cyan-emitting applications, *CrystEngComm*, 2021, **23**(44), 7805–7812.

30 Y. B. Xue, Y. Y. Shan and H. Xu, First-principles study on the initial decomposition process of $CH_3NH_3PbI_3$, *J. Chem. Phys.*, 2017, **147**(12), DOI: **10.1063/1.4995496**.

31 P. Ramasamy, D. H. Lim, B. Kim, S. H. Lee, M. S. Lee and J. S. Lee, All-inorganic cesium lead halide perovskite nanocrystals for photodetector applications, *Chem. Commun.*, 2016, **52**(10), 2067–2070.

32 J. F. Yuan, L. X. Zhang, C. H. Bi, M. R. Wang and J. J. Tian, Surface Trap States Passivation for High-Performance Inorganic Perovskite Solar Cells, *Solar Rrl*, 2018, **2**(10), DOI: **10.1002/solr.201800188**.

33 Y. Shen, H. Y. Wu, Y. Q. Li, K. C. Shen, X. Y. Gao, F. Song and J. X. Tang, Interfacial Nucleation Seeding for Electroluminescent Manipulation in Blue Perovskite Light-Emitting Diodes, *Adv. Funct. Mater.*, 2021, **31**(45), DOI: **10.1002/adfm.202103870**.

34 W. Li, Z. M. Wang, F. Deschler, S. Gao, R. H. Friend and A. K. Cheetham, Chemically diverse and multifunctional hybrid organic–inorganic perovskites, *Nat. Rev. Mater.*, 2017, **2**(3), DOI: **10.1038/natrevmats.2016.99**.

35 C. Chen, T. Han, S. Tan, J. J. Xue, Y. P. Zhao, Y. F. Liu, H. R. Wang, W. Hu, C. Bao, M. Mazzeo, R. Wang, Y. Duan and Y. Yang, Efficient Flexible Inorganic Perovskite Light-Emitting Diodes Fabricated with $CsPbBr_3$ Emitters Prepared via Low-Temperature in Situ Dynamic Thermal Crystallization, *Nano Lett.*, 2020, **20**(6), 4673–4680.

36 S. Laalioui, K. B. Alaoui, H. A. Dads, K. El Assali, B. Ikken and A. Outzourhit, Progress in perovskite based solar cells: scientific and engineering state of the art, *Rev. Adv. Mater. Sci.*, 2020, **59**(1), 10–25.

37 K. X. Chen, X. L. Zhang, P. A. Chen, J. Guo, M. He, Y. Q. Chen, X. C. Qiu, Y. Liu, H. J. Chen, Z. B. Zeng, X. Wang, J. Y. Yuan, W. L. Ma, L. Liao, T. Q. Nguyen and Y. Y. Hu, Solution-Processed $CsPbBr_3$ Quantum Dots/Organic Semiconductor Planar Heterojunctions for High-Performance Photodetectors, *Adv. Sci*, 2022, DOI: **10.1002/advs.202105856**.

38 F. Q. Meng, B. C. Yu, Q. H. Zhang, Y. Q. Cui, S. Tan, J. J. Shi, L. Gu, D. M. Li, Q. B. Meng and C. W. Nan, Ge Incorporation to Stabilize Efficient Inorganic $CsPbI_3$ Perovskite Solar Cells, *Adv. Energy Materi.*, 2022, **12**(10), DOI: **doi.org/10.1002/aenm.202103690**.

39 E. P. Yao, Z. L. Yang, L. Meng, P. Y. Sun, S. Q. Dong, Y. Yang and Y. Yang, High-Brightness Blue and White LEDs based on Inorganic Perovskite Nanocrystals and their Composites, *Adv. Mater.*, 2017, **29**(23), DOI: **10.1002/adma.201606859**.

40 N. J. Jeon, J. H. Noh, W. S. Yang, Y. C. Kim, S. Ryu, J. Seo and S. I. Seok, Compositional engineering of perovskite materials for high-performance solar cells, *Nature*, 2015, **517**(7535), 476–480.

41 J. A. Schwenzer, T. Hellmann, B. A. Nejand, H. Hu, T. Abzieher, F. Schackmar, I. M. Hossain, P. Fassl, T. Mayer, W. Jaegermann, U. Lemmer and U. W. Paetzold, Thermal Stability and Cation Composition of Hybrid Organic–Inorganic Perovskites, *ACS Appl. Mater. Interfaces*, 2021, **13**(13), 15292–15304.

42 S. K. Karunakaran, G. M. Arumugam, W. T. Yang, S. J. Ge, S. N. Khan, Y. H. Mai, X. Z. Lin and G. W. Yang, Europium(II)-Doped All-Inorganic $CsPbBr_3$ Perovskite Solar Cells with Carbon Electrodes, *Solar Rrl*, 2020, **4**(11), DOI: **10.1002/solr.202000390**.

43 M. T. Weller, O. J. Weber, J. M. Frost and A. Walsh, Cubic Perovskite Structure of Black Formamidinium Lead Iodide, alpha- $HC(NH_2)_{(2)}PbI_3$, at 298 K, *J. Phys. Chem. Lett.*, 2015, **6**(16), 3209–3212.

44 M. Kulbak, S. Gupta, N. Kedem, I. Levine, T. Bendikov, G. Hodes and D. Cahen, Cesium Enhances Long-Term Stability of Lead Bromide Perovskite-Based Solar Cells, *J. Phys. Chem. Lett.*, 2016, **7**(1), 167–172.

45 T. Guner, G. Topcu, U. Savaci, A. Genc, S. Turan, E. Sari and M. M. Demir, Polarized emission from $CsPbBr_3$ nanowire embedded-electrospun PU fibers, *Nanotechnology*, 2018, **29**(13), DOI: **10.1088/1361-6528/aaaaef**.

46 X. Lu, Y. Hu, J. Z. Guo, C. F. Wang and S. Chen, Fiber-Spinning-Chemistry Method toward In Situ Generation of Highly Stable Halide Perovskite Nanocrystals, *Adv. Sci.*, 2019, **6**(22), DOI: **10.1002/advs.201901694**.

47 J. Xu, *Preparation of high-efficiency perovskite solar cells based on novel cavity transport materials*, MS thesis, Harbin Institute of Technology, 2020.

48 Y. Huang, Q. D. Sun, W. Xu, Y. He and W. J. Yin, Halide Perovskite Materials for Solar Cells: a Theoretical Review, *Acta Phys.-Chim. Sin.*, 2017, **33**(9), 1730–1751.

49 J. R. Zhang, G. Hodes, Z. W. Jin and S. Z. Liu, All-Inorganic $CsPbX_3$ Perovskite Solar Cells: Progress and Prospects, *Angew. Chem., Int. Ed.*, 2019, **58**(44), 15596–15618.

50 J. Z. Song, J. H. Li, X. M. Li, L. M. Xu, Y. H. Dong and H. B. Zeng, Quantum Dot Light-Emitting Diodes Based on Inorganic Perovskite Cesium Lead Halides ($CsPbX_3$), *Adv. Mater.*, 2015, **27**(44), 7162–7167.

51 X. M. Li, Y. Wu, S. L. Zhang, B. Cai, Y. Gu, J. Z. Song and H. B. Zeng, $CsPbX_3$ Quantum Dots for Lighting and Displays: Room-Temperature Synthesis, Photoluminescence Superiorities, Underlying Origins and White Light-Emitting Diodes, *Adv. Funct. Mater.*, 2016, **26**(15), 2435–2445.

52 J. R. Zhu, X. L. Yang, Y. H. Zhu, Y. W. Wang, J. Cai, J. H. Shen, L. Y. Sun and C. Z. Li, Room-Temperature Synthesis of Mn-Doped Cesium Lead Halide Quantum Dots with High Mn Substitution Ratio, *J. Phys. Chem. Lett.*, 2017, **8**(17), 4167–4171.

53 Y. Su, X. J. Chen, W. Y. Ji, Q. H. Zeng, Z. Y. Ren, Z. S. Su and L. Liu, Highly Controllable and Efficient Synthesis of Mixed-Halide $CsPbX_3$ (X = Cl, Br, I) Permiskite QDs toward the Tunability of Entire Visible Light, *ACS Appl. Mater. Interfaces*, 2017, **9**(38), 33020–33028.

54 W. W. Chen, X. S. Tang, Z. G. Zang, Y. Shi, Z. Q. Yang and J. Du, Tunable dual emission in Mn^{2+}-doped $CsPbX_3$ (X = Cl, Br) quantum dots for high efficiency white light-emitting diodes, *Nanotechnology*, 2019, **30**(7), DOI: **10.1088/1361-6528/aaf299**.

55 Q. Y. Zhang, F. Y. Diao, X. Y. Xue, X. L. Sheng, D. Barba and Y. Q. Wang, Self-Assembly of $CsPbBr_3$ Nanocubes into 2D Nanosheets, *ACS Appl. Mater. Interfaces*, 2021, **13**(37), 44777–44785.

56 M. Jagadeeswararao, P. Vashishtha, T. J. N. Hooper, A. Kanwat, J. W. M. Lim, S. K. Vishwanath, N. Yantara, T. Park, T. C. Sum, D. S. Chung, S. G. Mhaisalkar and N. Mathews, One-Pot Synthesis and Structural Evolution of Colloidal Cesium Lead Halide-Lead Sulfide Heterostructure Nanocrystals for Optoelectronic Applications, *J. Phys. Chem. Lett.*, 2021, **12**(39), 9569–9578.

57 Y. Tong, Q. Wang, E. R. Mei, X. J. Liang, W. Gao and W. D. Xiang, One-Pot Synthesis of $CsPbX_3$ (X = Cl, Br, I)@Zeolite: A Potential Material for Wide-Color-Gamut Backlit Displays and Upconversion Emission, *Adv. Opt. Mater.*, 2021, **9**(11), DOI: **10.1002/adom.202100012**.

58 Y. Hu, Q. Wang, Y. L. Shi, M. Li, L. Zhang, Z. K. Wang and L. S. Liao, Vacuum-evaporated all-inorganic cesium lead bromine perovskites for high-performance light-emitting diodes, *J. Mater. Chem. C*, 2017, **5**(32), 8144–8149.

59 L. Zhang, F. Yuan, H. Dong, B. Jiao, W. W. Zhang, X. Hou, S. F. Wang, Q. H. Gong and Z. X. Wu, One-Step Co-Evaporation of All-Inorganic Perovskite Thin Films with Room-Temperature Ultralow Amplified Spontaneous Emission Threshold and Air Stability, *ACS Appl. Mater. Interfaces*, 2018, **10**(47), 40661–40671.

60 T. Burwig, W. Franzel and P. Pistor, Crystal Phases and Thermal Stability of Co-evaporated $CsPbX_3$ (X = I, Br) Thin Films, *J. Phys. Chem. Lett.*, 2018, **9**(16), 4808–4813.

61 P. P. Du, J. H. Li, L. Wang, J. Liu, S. R. Li, N. Liu, Y. X. Li, M. Y. Zhang, L. Gao, Y. Ma and J. Tang, Vacuum-Deposited Blue Inorganic Perovskite Light-Emitting Diodes, *ACS Appl. Mater. Interfaces*, 2019, **11**(50), 47083–47090.

62 M. Shin, H. S. Lee, Y. C. Sim, Y. H. Cho, K. C. Choi and B. Shin, Modulation of Growth Kinetics of Vacuum-Deposited $CsPbBr_3$ Films for Efficient Light-Emitting Diodes, *ACS Appl. Mater. Interfaces*, 2020, **12**(1), 1944–1952.

63 H. M. Ghaithan, S. M. H. Qaid, Z. A. Alahmed, M. Hezam, A. Lyras, M. Amer and A. S. Aldwayyan, Anion Substitution Effects on the Structural, Electronic, and Optical Properties of Inorganic $CsPb(I_{1-x}Br_x)(3)$ and $CsPb(Br_{1-x}Cl_x)(3)$ Perovskites: Theoretical and Experimental Approaches, *J. Phys. Chem. C*, 2021, **125**(1), 886–897.

64 S. Ullah, P. X. Yang, Y. Q. Li, J. M. Wang, L. L. Liu, R. Mahmood, S. E. Yang, T. Y. Xia, H. Z. Guo and Y. S. Chen, Two step vapor-processing and experimental investigations of all-inorganic $CsPbCl_3$ perovskite films for optoelectronic applications, *Mater. Lett.*, 2021, 294.

65 M. S. Yang, J. Yu, S. Z. Jiang, C. Zhang, Q. Q. Sun, M. H. Wang, H. Zhou, C. H. Li, B. Y. Man and F. C. Lei, High stability luminophores: fluorescent $CsPbX_3$ (X = Cl, Br and I) nanofiber prepared by one-step electrospinning method, *Opt. Express*, 2018, **26**(16), 20649–20660.

66 L. H. Zhang, Q. S. Sun, Y. K. Xu, L. L. Han, Q. Wang, Y. C. Yu, Z. W. Jin, S. K. Yang and Z. P. Ci, Self-assembled template-confined growth of ultrathin $CsPbBr_3$ nanowires, *Appl. Mater. Today*, 2020, 18.

67 Y. J. Huang, T. T. Wang, J. Z. Zheng, F. M. Li, W. R. Lan, F. Y. Zheng and S. X. Li, Multiwalled Carbon Nanotubes/$CsPbX_3$@Polyacrylonitrile Core/Shell Nanofibers with Ultrahigh Water, Thermal, and Ultraviolet Stability, *Macromol. Mater. Eng.*, 2021, **306**(10), DOI: **10.1002/mame.202100200**.

68 W. N. Liu, H. Fu, H. Liao, Z. Liang, Y. M. Ye, J. J. Zheng and W. Y. Yang, In situ synthesis of coaxial $CsPbX_3$@polymer (X

= Cl, Br, I) fibers with significantly enhanced water stability, *J. Mater. Chem. C*, 2020, **8**(40), 13972–13975.

69 J. H. Cha, H. Kim, Y. Lee, S. J. Kim, M. W. Lee, J. Kim and D. Y. Jung, Nanoscale optical imaging of perovskite nanocrystals directly embedded in polymer fiber, *Compos. Sci. Technol.*, 2019, 181.

70 K. J. Babu, G. Kaur, L. Biswal, G. De and H. N. Ghosh, Ultrafast Charge Delocalization Dynamics of Ambient Stable $CsPbBr_3$ Nanocrystals Encapsulated in Polystyrene Fiber, *Chem. – Eur. J.*, 2021, **27**(2), 683–691.

71 S. Chan, M. N. Liu, K. Latham, M. Haruta, H. Kurata, T. Teranishi and Y. Tachibana, Monodisperse and size-tunable PbS colloidal quantum dots via heterogeneous precursors, *J. Mater. Chem. C*, 2017, **5**(8), 2182–2187.

72 J. Yao, *All-Inorganic Lead Halide Perovskite Efficient Light Emitting Nanocrystals and Light Emitting Diode Devices*, PhD thesis, University of Science and Technology of China, 2021.

73 W. W. Yu and X. G. Peng, Formation of high-quality CdS and other II–VI semiconductor nanocrystals in noncoordinating solvents: Tunable reactivity of monomers, *Angew. Chem., Int. Ed.*, 2002, **41**(13), 2368–2371.

74 A. Yan, *Preparation, optical properties and LED applications of all-inorganic halide perovskite*, PhD thesis, Wuhan University of Technology, 2020.

75 J. Fu, *Shape control and its application in electrostatic spinning*, PhD thesis, Lanzhou University, 2014.

76 S. He, *Analysis and validation of the factors influencing the morphology of electrostatically spun nanofibers*, PhD thesis, Donghua University, 2011.

77 L. B. Qiu, J. Deng, X. Lu, Z. B. Yang and H. S. Peng, Integrating Perovskite Solar Cells into a Flexible Fiber, *Angew. Chem., Int. Ed.*, 2014, **53**(39), 10425–10428.

78 Z. L. Zhang, Z. H. Chen, J. B. Zhang, W. J. Chen, J. F. Yang, X. M. Wen, B. Wang, N. Kobamoto, L. Yuan, J. A. Stride, G. J. Conibeer, R. J. Patterson and S. J. Huang, Significant Improvement in the Performance of PbSe Quantum Dot Solar Cell by Introducing a $CsPbBr_3$ Perovskite Colloidal Nanocrystal Back Layer, *Adv. Energy Mater.*, 2017, **7**(5), DOI: **10.1002/aenm.201601773**.

79 H. L. Wang, Z. J. Dong, H. C. Liu, W. P. Li, L. Q. Zhu and H. N. Chen, Roles of Organic Molecules in Inorganic $CsPbX_3$ Perovskite Solar Cells, *Adv. Energy Mater.*, 2021, **11**(1), DOI: **10.1002/aenm.202002940**.

80 Q. W. Zhou, J. L. Duan, J. Du, Q. Y. Guo, Q. Y. Zhang, X. Y. Yang, Y. Y. Duan and Q. W. Tang, Tailored Lattice ''Tape'' to Confine Tensile Interface for 11.08%-Efficiency All-Inorganic $CsPbBr_3$ Perovskite Solar Cell with an Ultrahigh Voltage of 1.702 V, *Adv. Sci.*, 2021, **8**(19), DOI: **10.1002/advs.202101418**.

81 C. K. Ng, W. P. Yin, H. C. Li and J. J. Jasieniak, Scalable synthesis of colloidal $CsPbBr_3$ perovskite nanocrystals with high reaction yields through solvent and ligand engineering, *Nanoscale*, 2020, **12**(8), 4859–4867.

82 Z. Z. Li, B. Ma, Y. K. Xu, Y. T. Lei, W. Lan, G. Wang, W. Q. Li, Q. Wang, H. L. Zhang and Z. W. Jin, N-methyl-2-pyrrolidone Iodide as Functional Precursor Additive for Record Efficiency 2D Ruddlesden-Popper $(PEA)_{(2)}(Cs)_{(n)-1}Pb_nI_{3n+1}$ Solar Cells, *Adv. Funct. Mater.*, 2021, **31**(52), DOI: **10.1002/adfm.202106380**.

83 H. X. Rao, S. Y. Ye, F. D. Gu, Z. R. Zhao, Z. W. Liu, Z. Q. Bian and C. H. Huang, Morphology Controlling of All-Inorganic Perovskite at Low Temperature for Efficient Rigid and Flexible Solar Cells, *Adv. Energy Mater.*, 2018, **8**(23), DOI: **10.1002/aenm.201800758**.

84 J. Liang, X. Han, J. H. Yang, B. Y. Zhang, Q. Y. Fang, J. Zhang, Q. Ai, M. M. Ogle, T. Terlier, A. A. Marti and J. Lou, Defect-Engineering-Enabled High-Efficiency All-Inorganic Perovskite Solar Cells, *Adv. Mater.*, 2019, **31**(51), DOI: **10.1002/adma.201903448**.

85 C. Y. Duan, J. Cui, M. M. Zhang, Y. Han, S. M. Yang, H. Zhao, H. T. Bian, J. X. Yao, K. Zhao, Z. K. Liu and S. Z. Liu, Precursor Engineering for Ambient-Compatible Antisolvent-Free Fabrication of High-Efficiency $CsPbI_2Br$ Perovskite Solar Cells, *Adv. Energy Mater.*, 2020, **10**(22), DOI: **10.1002/aenm.202000691**.

86 C. Gao, Z. Y. Hu, C. Yang, H. Y. Xu, Y. Y. Wang, H. C. Zhang, J. Zhang, Y. J. Zhu and J. Wang, High-temperature induced iodide and bromide ions filling lattice for high efficient all-inorganic perovskite solar cells, *J. Alloys Compd.*, 2020, 848.

87 J. F. Liao, W. G. Li, H. S. Rao, B. X. Chen, X. D. Wang, H. Y. Chen and D. B. Kuang, Inorganic cesium lead halide $CsPbX_3$ nanowires for long-term stable solar cells, *Sci. China: Mater.*, 2017, **60**(4), 285–294.

88 J. W. Chen, H. Y. Xiang, J. Wang, R. Wang, Y. Li, Q. S. Shan, X. B. Xu, Y. H. Dong, C. T. Wei and H. B. Zeng, Perovskite White Light Emitting Diodes: Progress, Challenges, and Opportunities, *ACS Nano*, 2021, **15**(11), 17150–17174.

89 Y. F. Miao, X. M. Liu, Y. T. Chen, T. Y. Zhang, T. F. Wang and Y. X. Zhao, Deep-Red Perovskite Light-Emitting Diodes Based on One-Step-Formed gamma-$CsPbI_3$ Cuboid Crystallites, *Adv. Mater.*, 2021, **33**(51).

90 S. M. Chen, C. Chen, C. Bao, M. Mujahid, Y. Li, P. Chen and Y. Duan, White Light-Emitting Devices Based on Inorganic Perovskite and Organic Materials, *Molecules*, 2019, **24**(4), DOI: **10.3390/molecules24040800**.

91 H. Yu, G. M. Tian, W. W. Xu, S. W. Wang, H. K. Zhang, J. Z. Niu and X. Chen, Green Light-Emitting Devices Based on Perovskite $CsPbBr_3$ Quantum Dots, *Front. Chem.*, 2018, 6.

92 J. C. Yu, A. Y. Lee, D. B. Kim, E. D. Jung, D. W. Kim and M. H. Song, Enhancing the Performance and Stability of Perovskite Nanocrystal Light-Emitting Diodes with a Polymer Matrix, *Adv. Mater. Technol.*, 2017, **2**(6), DOI: **10.1002/admt.201700003**.

93 C. Y. Zhang, B. Wang, W. L. Zheng, S. Q. Huang, L. Kong, Z. C. Li, G. F. He and L. Li, Hydrofluoroethers as orthogonal solvents for all-solution processed perovsknite quantum-dot light-emitting diodes, *Nano Energy*, 2018, **51**, 358–365.

94 F. G. Zhou, Z. Z. Li, W. Lan, Q. Wang, L. M. Ding and Z. W. Jin, Halide Perovskite, a Potential Scintillator for X-Ray Detection, *Small Methods*, 2020, **4**(10), DOI: **10.1002/smtd.202000506**.

95 X. M. Li, D. J. Yu, J. Chen, Y. Wang, F. Cao, Y. Wei, Y. Wu, L. Wang, Y. Zhu, Z. G. Sun, J. P. Ji, Y. L. Shen, H. D. Sun and H. B. Zeng, Constructing Fast Carrier Tracks into Flexible Perovskite Photodetectors To Greatly Improve Responsivity, *ACS Nano*, 2017, **11**(2), 2015–2023.

96 H. Liu, X. W. Zhang, L. Q. Zhang, Z. G. Yin, D. G. Wang, J. H. Meng, Q. Jiang, Y. Wang and J. B. You, A high-performance photodetector based on an inorganic perovskite-ZnO heterostructure, *J. Mater. Chem. C*, 2017, **5**(25), 6115–6122.